Dynamic Coupling Phenomena in Molecular Excited States. III. Associative Ionization and Dissociative Recombination in H_2

Svend Erik Nielsen
Chemistry Laboratory III, *H. C. Ørsted Institute*,
University of Copenhagen, 2100 *Copenhagen*, *Denmark*

and

R. Stephen Berry
Department of Chemistry and The James Franck Institute,
University of Chicago, *Chicago*, *Illinois* 60637

(Received 28 September 1970)

A detailed calculation based on a perturbed stationary-state description is presented for associative ionization of hydrogen atoms. Specific rate constants $k_{AI}(v, K, T)$ are evaluated for the set of electronic states correlating with $H(n=1)+H(n=3)$ for associative ionization into vibrational ($v=0-8$) and rotational ($K=0-21$) states of $H_2^+(X^2\Sigma_g^+)$ at $T=300$ °K and at $T=600$ °K. Cross sections $Q_{AI}(v, K, E)$ are given for the most significant electronic state, the $(1s\sigma, 4s\sigma)$ united atom configuration, and, by microscopic reversibility, cross sections for the reverse reaction, dissociative recombination, are obtained. Cross sections for associative ionization at thermal energies, $Q_{AI}(v, K, 10^{-3}$ a.u.), are at most of a magnitude about 10^{-18} cm^2. Corresponding specific rate constants, $k_{AI}(v, K, 300$ °K), fall in the range 10^{-14}–10^{-13} cm^3/sec and display a temperature dependence $k_{AI}(T) \propto T^{-0.33}$. Dissociative recombination cross sections, $Q_{DR}(v, K, 10^{-3}$ a.u.), are obtained for the $v=4-8$ vibrational states, with magnitudes about 10^{-16} cm^2. The resulting specific rate constants, $k_{DR}(v, K, 300$ °K), are at most 10^{-10} cm^3/sec and display a temperature dependence $k_{DR}(T_e) \propto T_e^{-1/2}$ for $T_e \lesssim 80$ °K, $k_{DR}(T_e) \propto T_e^{-0.75}$ for $T_e \approx 300$ °K, and a still larger-power decrease for increasing T_e at $T_e > 300$ °K.

I. INTRODUCTION

In Paper I of this series[1] we have described a general method to analyze vibrational-electronic coupling phenomena. Our aim so far has been to use H_2 as a model system to study the microscopic origins of vibronic perturbations in Rydberg states,[1] and to investigate the competing coupling processes of autoionization and predissociation.[2] It is the purpose of this paper to apply the method, utilizing its stationary-state basis functions for the complete particle system, to the processes of associative ionization (AI) and dissociative recombination (DR) as induced by vibronic coupling:

$$H(1s) + H^*(n=3) \underset{DR}{\overset{AI}{\rightleftharpoons}} H_2^+(^2\Sigma_g^+, v, K) + e \ . \qquad (1)$$

Our treatment will be restricted to the energetically lowest AI channels open in the thermal-energy range, i.e., to excited hydrogen atoms of principal quantum number $n=3$, and we shall examine DR only in the same channels. Our main object will be to obtain reaction cross sections and specific rates as functions of energy and temperature, respectively, and as functions of the molecular electronic states and the vibrational and the rotational states of the hydrogen molecular ion. A preliminary account of parts of this work has been given.[3] We shall see that the theoretical description of vibronically induced AI and DR processes, as exemplified by (1), gives results entirely consistent with currently available data for these processes in hydrogen, and gives a general account of the temperature dependence to be expected for AI and DR.

The experimental evidence and general theoretical considerations indicate that cross sections for AI and DR are several orders of magnitude smaller for hydrogen and helium than for the better-studied oxygen, nitrogen, and nitric oxide systems. This difference appears to be due to a basic difference in the mechanisms by which bound and free electronic states are coupled. In oxygen, nitrogen, and nitric oxide, the possibility exists for coupling via electron-electron correlation, even in collisions at thermal energies. H_2 and He_2 have such simple electronic structures that their electronic degrees of freedom cannot provide the requisite coupling energy in thermal collisions. To interpret AI and DR in hydrogen and helium, one must call upon the next most effective coupling mechanism, viz., vibrational-electronic, to deal with thermal collisions, or one must go to systems at 10^4 °K in order to invoke electron correlation as the coupling mechanism. Further on in this section, this comparison is made in more detail.

The maximum rates ν_{el}, associated with coupling by electron correlation, compare with the maximum rates ν_{vib}, associated with vibrational-electronic coupling, roughly as the Bohr period compares

with a vibrational frequency—about 10^3 faster. Hence it is no surprise that recombination coefficients for helium and hydrogen are three or four orders of magnitude smaller than those of the heavier gases. It is important to bear in mind that the numerical results of this investigation are appropriate only when the vibrational-electronic mechanism is the dominant one. Nevertheless, the general formulation of the problem is applicable whatever the coupling mechanism. One need only replace the nuclear kinetic-energy operator, appropriate for vibrational-electronic coupling, with the difference between the electron-electron interaction potential and the Hartree-Fock potential, in order to deal with the mechanism as it is usually invoked. [4,5]

Although the magnitudes differ, it is expected that the *general forms* derived here for the dependence of cross sections on energy, and on vibrational and rotational state, and of the rate coefficients on temperature, will hold for electronically coupled cases, because most of the general characteristics governing the T matrix for vibronic coupling hold for the T matrix of electronic coupling as well. Some caution is necessary in making this extension, because, at least according to popular dogma, AI and DR in the heavier systems are dominated by transitions at curve crossings. By contrast, the vibronically coupled light-atom systems accumulate transition amplitude over large ranges of internuclear separation, and do not depend on curve crossings.

To put the problem in perspective, it is useful to review the current experimental and theoretical situation with regard first to DR and then to AI. Special emphasis is given to the simpler systems, hydrogen and helium.

The experimental interest (aeronomy and laboratory plasma physics) in electron recombination by DR dates back two decades and essentially was stimulated by Bates, [4] who pointed out that DR is a very effective mode of electron recombination as opposed to competing mechanisms, for example, radiative recombination and collisional-radiative recombination. The significance of DR is now well established for the inert gases, with the exception of helium, as well as for the molecular ions of aeronomic interest, O_2^+, N_2^+, and NO^+. Most rate coefficients for dissociative recombination are of the order 10^{-7}–10^{-6} cm^3/sec at 300 °K. [5] The temperature dependence of DR is still uncertain, but the apparent discrepancies seem to be due largely to varying experimental conditions. [6] The DR specific rate may be expressed as an inverse power of temperature, $k \sim T_e^{-\gamma}$, γ being about 0.4–0.7 if T_e is the electron temperature, [6] and quite often an over-all $T^{-3/2}$ dependence has been reported. For helium [7] and for hydrogen, [8] the experimental situation is less satisfactory; the accepted rates for DR in these systems have exhibited a rather steady monotonic downward trend. Early high estimates of these rates were reinterpreted in terms of competing gas-phase mechanisms and gas-surface reactions, and upper limits to the recombination coefficients were soon estimated to be no larger than 10^{-9}–10^{-8} cm^3/sec for these gases. More recent studies have moved these figures down much further; Robertson's investigations of the helium afterglow [9] have given a recombination coefficient as low as 2×10^{-11} cm^3/sec at $T_e = 1800$ °K and electron density 10^{12} cm^{-3}, and Collins and Robertson [10] have proposed the possibility of collisional dissociative recombination of electrons and molecular ions, later estimated by Collins [11] in a hypothetical model calculation to give recombination coefficients of just that order of magnitude. Ferguson *et al.* [12] have advocated a three-body collisional mechanism for recombination in helium, supported by findings of an electron temperature dependence stronger than $T_e^{-7/2}$, and their analysis of experimental data suggests about 3×10^{-10} cm^3/sec as an upper limit to the recombination coefficient of DR for helium. Recently the three-body collisional-radiative recombination has been invoked by Born [13] in the interpretation of helium afterglow experiments over an extended range of temperatures, the recombination coefficient being about equal to the theoretical one for the atomic ion, [14] i.e., 10^{-10}–10^{-9} cm^3/sec at electron densities 10^{12}–10^{13} cm^{-3} and electron temperatures $T_e \approx 10^3$ °K. For hydrogen no recent experimental results are available but the situation may be very much like the one encountered for helium. The experimental knowledge of DR for He_2^+ and H_2^+ thus appears to be quite limited; the recombination coefficients measured are probably due to three-body recombination of the atomic as well as the molecular ions and depend upon plasma densities. The conclusion that we may draw seems to be restricted to an order-of-magnitude upper bound for the specific rate of DR for He_2^+ at 10^{-10} cm^3/sec under the usual experimental conditions at 300 °K.

From a theoretical point of view we have good reasons to expect this situation for hydrogen and helium. Repulsive potential-energy curves of He_2 do not cross the ground-state curve of He_2^+ in the region of the lowest vibrational state, [15] which is the generally accepted requirement for DR to occur at low temperatures. Quantitatively, however, theory so far has given little information about the details of a DR mechanism, although a number of formal approaches have been described in the literature. [16–18] The early calculations of DR rates by Bates [4] and Bauer and Wu [19] are essentially semiquantitative estimates to justify the magnitudes of the then-accepted experimental rates, which now

seem to be too high. The model calculation of DR for H_2^+ by Bauer and Wu was later repeated by Wilkins,[20] who invoked a Monte-Carlo technique for integral evaluation, and the results of Bauer and Wu were regained at energies below 1 eV, giving a recombination coefficient at 3×10^{-8} cm^3/sec. More recently, Warke, using noncrossing potential-energy curves,[21] has made a semiclassical model calculation of DR rates for O_2^+, N_2^+, and He_2^+. The model was later refined by Chan[22] in a calculation of DR for O_2^+ that assumed the usual favorable crossing of the potential-energy curves. The results of Warke for O_2^+ and N_2^+ are in reasonable agreement with experiments, but Chan[22] and Bardsley[23] have pointed out that the approximations involved lead to overestimation of DR rates, and the result for He_2^+, 2×10^{-8} cm^3/sec, certainly appears too large by order(s) of magnitude. Dubrovsky, Ob'edkov, and Janev[24] report a quantum-mechanical calculation of DR for H_2^+ *assuming* a crossing of the H_2^+ ground state and an intermediate H_2 resonance state $(2p\sigma_u)^2\,{}^1\Sigma_g^+$. The specific rate obtained is $42\times10^{-8}\times T^{1/2}$ cm^3/sec, again however an "upper-bound" result that probably does not hold for the system in question. Bardsley[23] has proposed an indirect mode of DR, involving a resonance Rydberg state of the neutral molecule, and estimates of rates of the direct and indirect modes of DR have been obtained for NO^+ by incorporation of spectroscopic data in a resonance scattering theory. The results indicate that the indirect mode may be important whenever the energy band of about kT below the ionic dissociation limit contains Rydberg states that decay faster by predissociation than by autoionization. The temperature dependence of the indirect mode is estimated as $T^{-3/2}$, which is appreciably stronger than that of the direct mode $T^{-1/2}$, and the author suggests the presence of both modes of DR as an explanation of the controversy over temperature dependences. A discussion of the experimental temperature dependence of DR has very recently been given by O'Malley,[25] who takes into account specifically two characteristic temperatures, T_e for the electrons and T_v for the molecular ion. For favorable curve crossing in the region of the vibrational ground state of the ion (according to O'Malley, a "maximal system"), simple considerations indicate a specific rate $k(T_e,\ T_v)\sim T_e^{-1/2}(1-e^{-h\nu/kT_v})$, $h\nu$ being the vibrational spacing, when DR from the vibrationally excited states may be neglected. Thus at low T_v one has $k\sim T_e^{-1/2}$, whereas at high T_v ($kT_v \gg h\nu$), $k\sim T_e^{-1/2}T_v^{-1}$, and it is apparent how varying experimental conditions may result in temperature dependences from $T^{-1/2}$ to $T^{-3/2}$. If the rates from higher vibrational states may not be neglected, in the case of a "nonmaximal system," for example, the experimental rate is determined by an average sum over specific rates and the temperature dependence may be quite dependent upon the details of the states involved. We shall discuss these aspects in the following calculation of DR cross sections $Q_{DR}(v,\ K,\ E)$ for hydrogen, which is presumably a nonmaximal system.

Associative ionization along with Penning ionization ($A^*+B\rightarrow A+B^++e$) are typical chemi-ionization processes; AI is often called the Hornbeck-Molnar process.[26] These processes probably represent two of the most important mechanisms for ion production in flames and other chemical systems, in shock-heated gas systems, and in the upper atmosphere (see, for example, recent reviews of the field[5,27]). AI for the inert gases has been investigated by mass-spectrometric analysis of ionization about and below threshold by several authors.[28] The experiments however yield only the product of the rate constant and the lifetime of the excited atom, and estimates of lifetimes lead to rather large rate constants, about 10^{-9}–10^{-8} cm^3/sec. Determinations of the lifetimes of the excited species in AI experiments have later been reported for He by Kaul, Seyfried, and Taubert,[29] resulting in a specific rate 2×10^{-10} cm^3/sec, and for Ar by Becker and Lampe,[30] resulting in a specific rate 2×10^{-9} cm^3/sec. Teter, Niles, and Robertson[31] have identified AI for He from energy levels of principal quantum number $n=3$, and they report at $T=400\,^\circ$K average cross sections of about 10^{-16}–10^{-15} cm^2, which is essentially in agreement with the result of Kaul *et al.* Experiments have given strong evidence for chemi-ionization by AI for a variety of atomic and molecular species, but only a few details of cross-section magnitudes and energy dependencies. Recently, Chupka, Russell, and Refaey[32] have studied AI of a hydrogen molecule and an excited hydrogen atom, $H_2+H^*\rightarrow H_3^++e$. The experiments were interpreted as giving cross sections that decreased with increasing energy at least as rapidly as $E^{-1/2}$, and the explanation was offered that a transition from an attractive H_3^* potential-energy curve is involved.

Information concerning AI cross sections and rates from theory is also scarce. The discussion given by Mulliken of the electronic states of helium led to the conclusion that although DR from the He_2^+ ground vibrational state had to play a minor role, DR from the higher vibrational states might well be significant and thus also AI into these states for excited atoms of principal quantum number $n\geq3$. The appearance-potential investigations of He ionization[30,33] have indicated just that. In a recent discussion, Nielsen and Dahler[16] have emphasized these conclusions for hydrogen as well, and suggest that AI in hydrogen may occur at low temperatures mainly in exothermic channels, i.e., along attractive potential-energy curves, from the

$n=3$ atomic state. Some information about the AI mechanism may be extracted by analogy from a related reaction, associative detachment, i.e., for hydrogen $H+H^- \rightarrow H_2+e$, recently examined by Chen and Peacher[34] in a detailed calculation giving cross sections $Q_{AD}(v, K, E)$ as a function of initial kinetic energy, and vibrational-rotational state of the product molecule. Cross sections at a few eV are in the range 10^{-23}–10^{-22} cm^2, increasing strongly for decreasing E, for example, about 10^{-19} cm^2 for $v=3$, $K=0$–10, $E\approx 1$ eV, and weakly decreasing in an oscillatory fashion for increasing E in the range $E=3$–10 eV. We shall discuss these results in more detail in a comparison with the results of the present calculation for $Q_{AI}(v, K, E)$.

The roles of AI and DR in hydrogen and helium are still quite uncertain. In order to try to resolve these questions, as well as to probe further into the coupling of bound and free states in molecules, we have undertaken this rather detailed theoretical study of AI and DR in hydrogen. Our emphasis here is almost entirely on the states and mechanisms responsible for these processes in gases at temperatures of order 10^3 °K or cooler, and not on the rates and mechanisms that pertain in collisions with eV of relative energy. The differences between these situations are important to recognize, both for the light-atom cases in their own right, and because the thermal AI and DR of heavier systems such as nitrogen, oxygen, and nitric oxide probably correspond to the light-particle behavior at high energies. We can examine these differences by considering the potential curves of H_2.

In recent years, very extensive variational calculations have given some knowledge of the lower excited states of hydrogen over a range of internuclear distances, notably through the work of Davidson,[35] and Kolos,[36] and Kolos and Wolniewicz.[37–40] A discussion of known potential-energy curves of H_2 in relation to AI and DR mechanisms was given previously.[16] It is valuable to amplify this discussion now.

The hydrogen molecule exhibits a manifold of singly excited states based on $H_2^+(1\sigma_g)$ plus one more bound electron; these states are bonding states with potential wells that are essentially parallel with the potential well of H_2^+ itself, particularly for states in which the excited electron has a Rydberg quantum number $n\gtrsim 4$. This manifold of bonding states has been examined in detail in Refs. 1 and 2; the lower states of this manifold dominate AI and DR at thermal energies in H_2, and are our principal concern here. In particular, states dissociating to $H(1s)+H(3l)$, $l=0$, 1, 2, will be seen to be the most important for AI and DR of H_2 at thermal energies. Bonding states dissociating to $H(1s)+H(nl)$, $n\geq 4$, are similar to those giving an atom with $n=3$, but exhibit smaller cross sections and can be treated by scaling laws discussed previously.[1,2,41] Bonding states giving $H(1s)+H(2s, 2p)$ simply lie too far below the state $H_2^+ + e$ to play any role in thermal AI. Collisions of electrons with H_2^+ have been studied in the high-energy region,[42,43] and DR is found to play only a minor role.

In addition to the manifold of bonding states, H_2 also has a manifold of nonbonding states built on $H_2^+(1\sigma_u)$ plus a bound electron. These states, particularly those dissociating to $H(1s)+H(2s, 2p)$ and to $H(1s)+H(3l)$, would probably dominate AI and DR in H_2 in the high-temperature range, possibly starting as low as 2×10^3 °K, and extending upward as far as H_2 can exist. This can be seen by estimating where the repulsive curves for $H_2^*(1\sigma_u, 2l)$ and $H_2^*(1\sigma_u, 3l)$ cross the curve for $H_2^+(1\sigma_g)+e$. Presumably, according to the rapid Bates mechanism,[4] coupling of the H_2^* in these repulsive states with $H_2^+ + e$ can only take place in the vicinity of a crossing point (although the long de Broglie wavelength of hydrogen would make it the most likely of all atomic species to deviate from the crossing-point requirement). The repulsive states dissociating to $H(1s)+H(2s, 2p)$ cross the potential curve of H_2^+ with R in the vicinity of 3.8 bohr; 2.5 eV of kinetic energy are required for $H_{1s}+H(2s, 2p)$ to reach this point, in a head-on collision, to produce AI; this is far beyond the range available in thermal collisions, but is certainly accessible in high-energy collisions. To produce DR by coupling at this crossing point, H_2^+ must be in a vibrational state $v\sim 7$. This state is over 1.7 eV above the bottom of the potential well of H_2^+, and is virtually unpopulated at temperatures at which H_2^+ can exist.[44] (Admittedly, the present calculations for DR into bonding states of H_2^* do treat vibrational states of H_2^+ as high as $v=7$. This will eventually permit us to compare the rates of DR into bonding states by vibronic coupling, with the rates of DR into nonbonding states by electronic coupling—the Bates mechanism—or by vibronic coupling.)

The repulsive curves coming from $H(1s)+H(3l)$ cross the H_2^+ potential at an internuclear separation of about 4.7 bohr. To reach such a crossing point, over 0.76 eV are required, which means that the temperature of the system must be in the range 2–3000 °K if such collisions are to occur often enough to play a role in AI. For DR, H_2^+ must be in a vibrational state $v\sim 9$ if dissociation is to occur through the crossing point to give $H(1s)+H(3l)$. This is a sufficiently stringent constraint to make DR to $H(1s)+H(3l)$ along the *repulsive* curves quite unlikely to be observed under any conditions under which H_2^+ could exist. As a result of these conditions, we have concentrated on the manifold of bonding states of H_2 for the present. The role of the repulsive states and the mechanisms of their coupling will be the subject of another paper in

this series.

The repulsive states of H_2 have rough analogs in heavier molecules in the form of manifolds of states whose potential curves cross the ionic curves. Because the term manifolds of heavier molecules are so much richer in states, these molecules often exhibit crossings at energies only slightly above the energies of the corresponding dissociation limits. Furthermore, these crossings often occur near low vibrational levels of the ionic state, so that these crossings are available for both DR and AI in molecules such as NO.[23]

We have obtained (Paper I), including monopole and quadrupole terms in the expansion of the potential arising from an $H_2^+ (^2\Sigma_g^+)$ core, wave functions and energies for Rydberg states of H_2, and free ionic states $H_2^+ + e$ at internuclear distances $1 \leq R \leq 4$ a.u. The results for the over-all potential energy of each bound state were fitted to a modified Morse potential, and thus we have available a self-consistent and quite manageable description of the adiabatic electronic states and the corresponding potential-energy curves. Our model calculations compare well with respect to energetics with more refined calculations of H_2 Rydberg states and with experimental results, and the auto-ionization results[2] based on the energies and the wave functions lead to a general and quite good agreement with spectroscopic band identifications. We therefore feel that we are in a position to discuss AI and DR for hydrogen from a reasonably realistic point of view in a perturbed stationary-state calculation. Finally, with respect to the adiabatic scattering formulation, since we are interested neither in differential cross sections nor in exchange scattering, we keep the molecular frame of reference for the electrons at all internuclear distances, and we define total cross sections and specific rates for reaction in channels of specified molecular electronic states.

II. MODEL

In this section we give a summary of the basic assumptions in our description of the adiabatic electronic states, and we specify the simplifications of the reaction channels to be introduced to give a tractable scattering formulation.

We introduce a model Hamiltonian for use in the atomic as well as in the ionic channels of the reaction $H + H^* \rightarrow H_2^+ + e$, taking into account the variation with internuclear distance of the bound as well as the free electron states. We may thus describe initial and final states in terms of the *same* Hamiltonian, a model adiabatic (Born-Oppenheimer) Hamiltonian, and we shall consider transitions from atomic to ionic channels as only due to breakdown of the adiabatic approximation by vibronic coupling. To this end we have introduced the following simplifications.

We assume that the core electron follows the nuclear motion exactly. That is, we assume that the core electron is always in a $1s\sigma_g$ stationary state that is identical at each internuclear distance with the corresponding stationary electronic state of the hydrogen molecular ion, and independent of the state of the excited (free or bound) electron.

The outer electron moves in the field of two positive point charges (the protons at distance R) and a continuous negative-charge distribution of the $1s\sigma_g$ electron (we account for exchange in a modified Slater approximation). In a multipole expansion we determine an electron Hamiltonian (fixed R) in a molecular frame of reference,

$$\begin{aligned} H_e(\vec{r}, R) &= -\tfrac{1}{2}\nabla_{\vec{r}}^2 + V_{0cE}(r, R) + P_2(\cos\theta)\, V_{2c}(r, R) + \cdots \\ &= H_e^{(0)}(\vec{r}, R) + P_2(\cos\theta)\, V_{2c}(r, R) + \cdots \\ &= H_e^{(0)}(\vec{r}, R) + H_e^{(1)}(\vec{r}, R) + \cdots , \end{aligned} \tag{2}$$

giving rise, for example, to bound states

$$[H_e^{(0)}(\vec{r}, R) - \epsilon_{nl}^{(0)}(R)]\, \psi_{nl\Lambda}^{(0)}(\vec{r}, R) = 0 , \tag{3}$$

$$[H_e^{(0)}(\vec{r}, R) + H_e^{(1)}(\vec{r}, R) - \epsilon_{nl\Lambda}^{(1)}(R)]\, \psi_{nl\Lambda}^{(1)}(\vec{r}, R) = 0 , \tag{4}$$

$$\psi_{nl\Lambda}^{(1)}(\vec{r}, R) = \sum_{n'l'} a(nl, n'l', R)\, \psi_{n'l',\Lambda}^{(0)}(\vec{r}, R) . \tag{5}$$

We assume that nuclear angular momentum is conserved; that is, we neglect the rotational nuclear-electron coupling, and we describe the nuclear rotation in terms of spherical harmonics.

We shall consider the electrons always to be quantized in the molecular frame of reference.

We therefore state as good quantum numbers K, M, and Λ, where K and M refer to nuclear angular momentum in the laboratory system and Λ to the projection of electron angular momentum in the molecular system (the R component). Because of the inclusion of quadrupole terms in $H_e(\vec{r}, R)$, l is not a good quantum number, although it is nearly so for $np\sigma$ and $np\pi$ states. We do not express the uncoupling of electron motion with respect to $\vec{R}$ for $R \rightarrow \infty$ since we are interested neither in multiplet transitions nor exchange reactions resulting from the atom-atom collision.

Introducing the simplifications given above in the complete Hamiltonian for H_2 we may write our model Hamiltonian in the coordinates $\vec{R}$ and $\vec{r}$ of the nuclei and the outer electron ($\vec{r}$ in the molecular frame)

$$H_m = \frac{1}{m_H}\left(T_R + \frac{1}{R^2}\, K^2\right) + H_e(\vec{r}, R) + \frac{1}{R} + \epsilon_{1s\sigma_g}(R) , \tag{6}$$

where m_H is the mass of a hydrogen atom, T_R is the radial part of $\nabla_{\vec{R}}^2$, K is the nuclear (tumbling) angular momentum operator, and $\epsilon_{1s\sigma_g}(R)$ is the

H_2^+ core electron energy.

As our basic adiabatic set, we introduce according to our simplifications the functions

$$\Psi(\vec{r}, \vec{R}) = [\chi(R)/R]\, Y_K^M(\hat{\vec{R}})\, \psi_\Lambda(\vec{r}, R)\,, \tag{7}$$

where $\psi_\Lambda(\vec{r}, R)$ are bound- or free-electron wave functions obtained as eigenfunctions of $H_e(\vec{r}, R)$ in some approximation. We take quadrupole terms into account only for bound states $\psi_{n l\Lambda}^{(1)}(\vec{r}, R)$, and the free states are described by $\psi_{k l\Lambda}^{(0)}(\vec{r}, R)$. The functions $\Psi(\vec{r}, \vec{R})$ thus appear as eigenstates of H_m if we neglect the R dependence of the electronic states, i.e., define T_R as a Sternheimer operator

$$\left(T_R \frac{\chi(R)}{R}\right)\left(\frac{\chi(R)}{R}\right)^{-1},$$

and $\chi(R)$ results from the equation

$$\left[-\frac{d^2}{dR^2} + \frac{K(K+1)}{R^2} + m_H\left(\epsilon_e(R) + \epsilon_{1s\sigma_g}(R) + \frac{1}{R} - E\right)\right]\chi(R) = 0\,, \tag{8}$$

where $\epsilon_e(R)$ is obtained from $H_e\,\psi_\Lambda = \epsilon_e\,\psi_\Lambda$.

Two cases arise corresponding to atomic channels and to ionic channels of the system. If $\epsilon_e(R) = \epsilon_{n l\Lambda}^{(1)}(R)$ and the electron is in a bound state, we may determine nuclear free motion corresponding to total energy E in the potential

$$E_{n l\Lambda}(R) = \epsilon_{n l\Lambda}^{(1)}(R) + \epsilon_{1s\sigma}(R) + 1/R + 0.55556\,,$$

$$E = -0.55556 + [1/m_H]\, k_a^2\,,$$

i.e., free states $\chi_K(k_a, R)$ obtained from

$$\left[-\frac{d^2}{dR^2} + \frac{K(K+1)}{R^2} + m_H E_{n l\Lambda}(R) - k_a^2\right]\chi_K(k_a, R) = 0\,. \tag{8a}$$

If $\epsilon_e = \frac{1}{2} k_i^2$ (a.u.) and the electron is in a free state, we may determine bound nuclear states of total energy E in the potential

$$E(H_2^+, R) = \epsilon_{1s\sigma}(R) + 1/R\,,$$

$$E = E_{v,K} + \tfrac{1}{2} k_i^2\,,$$

i.e., bound states $\chi_{v,K}(R)$ obtained from

$$\left(-\frac{d^2}{dR^2} + \frac{K(K+1)}{R^2} + m_H\left[E(H_2^+, R) - E_{v,k}\right]\right)\chi_{v,k}(R) = 0\,, \tag{8b}$$

which are essentially the vibrational-rotational states of the hydrogen molecular ion.

The resulting potential-energy curves $E_{n l\Lambda}(R)$ for the hydrogen molecule were fitted to modified Morse potentials, and the results given in Paper I. An example of the energetics of the AI and DR channels is shown in Fig. 1.

We have presented in Paper I a general discussion of the bound-electron states $\psi_{n l\Lambda}^{(1)}(\vec{r}, R)$ and the corresponding energies $\epsilon_{n l\Lambda}^{(1)}(R)$ [Eqs. (4) and (5)], in particular, with respect to the l spoiling introduced by the quadrupole potential V_{2c} [Eq. (2)]. In the designation of the electron state, the quantum numbers nl refer to the united atom configuration, i.e., the mixing coefficients behave $a(nl, n'l', R) \to \delta_{nl,n'l'}$ for $R \to 0$. For increasing R, the states $\psi_{n l\Lambda}^{(0)}$, $n = 3, 4, 5, 6$, and $l = 1, 3$, do mix due to V_{2c}; however, the parentage of the states $\psi_{n l\Lambda}^{(1)}$ is still very definite in the region $0 < R < 4$ a.u., i.e., $a(nl, nl, R) > 0.97$ and the energies $\epsilon_{n l\Lambda}^{(1)}(R)$ are well separated. The $s\sigma$ and $d\sigma$ states, $l = 0, 2$ and $n = 3, 4, 5, 6$, on the other hand, mix very strongly in this region, in particular, for same principal quantum numbers, and the energies $\epsilon_{n s\sigma}^{(1)}(R)$ and $\epsilon_{n d\sigma}^{(1)}(R)$ display a crossing at $R_c \approx 2$ a.u. We have

$$\psi_{ns\sigma}^{(1)}(\vec{r}, R) = a(ns, ns, R)\,\psi_{ns\sigma}^{(0)}(\vec{r}, R) + a(ns, nd, R)\,\psi_{nd\sigma}^{(0)}(\vec{r}, R) + \sum_{n' \neq n}\sum_{l'=0,2}\cdots, \tag{9}$$

$$\psi_{nd\sigma}^{(1)}(\vec{r}, R) = a(nd, nd, R)\,\psi_{nd\sigma}^{(0)}(\vec{r}, R) - a(nd, ns, R)\,\psi_{ns\sigma}^{(0)}(\vec{r}, R) + \sum_{n' \neq n}\sum_{l'=0,2}\cdots, \tag{10}$$

where the mixing coefficients to a good approximation satisfy ($0 \leq R \leq 4$)

$$|a(ns, ns, R)|^2 + |a(ns, nd, R)|^2 \approx 1\,,$$

$$|a(nd, nd, R)|^2 + |a(nd, ns, R)|^2 \approx 1\,,$$

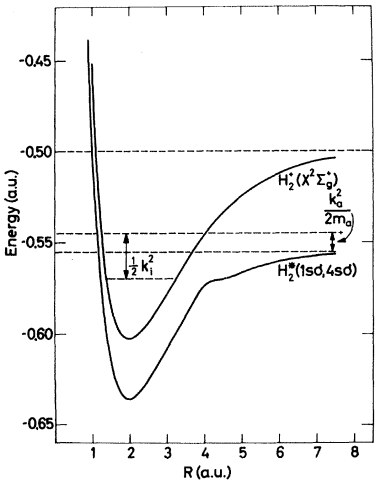

FIG. 1. Potential-energy curves exemplifying the energetics of AI-DR for hydrogen.

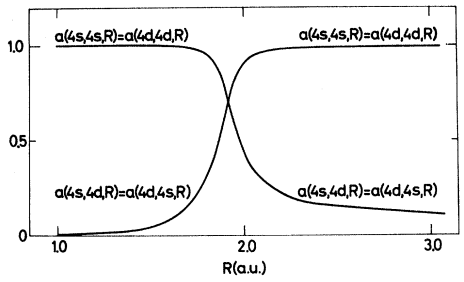

FIG. 2. Expansion coefficients $a(nl, nl', R)$ of the $4s\sigma_g$ and $4d\sigma_g$ states, Eqs. (9) and (10), in the strong-coupling region.

$$a(ns, ns, R) \approx a(nd, nd, R) ,$$

$$a(ns, nd, R) \approx a(nd, ns, R) , \tag{11}$$

and the energies satisfy the inequalities

$$\epsilon^{(1)}_{ns\sigma}(R) \lesssim \epsilon^{(1)}_{nd\sigma}(R) \quad \text{for } R \lesssim R_c . \tag{12}$$

We have listed in Table III B of Paper I the crossing energies for $n = 3, 4, 5, 6$ at $R = 1, 2, 3, 4$, a.u., and we take the opportunity to correct the $4s$ and $4d$ values at $R = 2$ a.u.: The entries should read -0.0330 and -0.0336, respectively. The behavior of the $4s$-$4d$ mixing coefficients in the crossing region is shown in Fig. 2, the crossing point at $R_c = 1.92$ a.u.

In the adiabatic limit however we choose the states that display an avoided crossing; i.e., states

$$\psi^{(1)}_{(ns)\sigma}(\vec{r}, R) = \begin{cases} \psi^{(1)}_{ns\sigma}(\vec{r}, R) , & R < R_c \\ a(nd, ns, R)\,\psi^{(0)}_{ns\sigma}(\vec{r}, R) + a(nd, nd, R)\,\psi^{(0)}_{nd\sigma}(\vec{r}, R), & R > R_c \end{cases} \tag{13}$$

$$\psi^{(1)}_{(nd)\sigma}(\vec{r}, R) = \begin{cases} \psi^{(1)}_{nd\sigma}(\vec{r}, R) , & R < R_c \\ a(ns, nd, R)\,\psi^{(0)}_{nd\sigma}(\vec{r}, R) - a(ns, ns, R)\,\psi^{(0)}_{ns\sigma}(\vec{r}, R) , & R > R_c \end{cases} \tag{14}$$

corresponding to noncrossing energies $\epsilon^{(1)}_{(ns)\sigma}(R) < \epsilon^{(1)}_{(nd)\sigma}(R)$ for all R:

$$\epsilon^{(1)}_{(ns)\sigma}(R) = \begin{cases} \epsilon^{(1)}_{ns\sigma}(R) & \text{for } R < R_c \\ \epsilon^{(1)}_{nd\sigma}(R) & \text{for } R > R_c , \end{cases} \tag{15}$$

$$\epsilon^{(1)}_{(nd)\sigma}(R) = \begin{cases} \epsilon^{(1)}_{nd\sigma}(R) & \text{for } R < R_c \\ \epsilon^{(1)}_{ns\sigma}(R) & \text{for } R > R_c . \end{cases} \tag{16}$$

When the adiabatic description is the pertinent one, we shall use the electronic states $\psi^{(1)}_{(nl)\sigma}$ and the over-all potential energy $E_{(nl)\sigma}(R) = \epsilon^{(1)}_{(nl)\sigma}(R) + \epsilon_{1s\sigma}(R) + 1/R + 0.55556$ for atomic channels of united atom configuration $ns\sigma$ and $nd\sigma$. The parametrized results $E_\alpha(R)$ of Paper I were all based upon the adiabatic noncrossing description.

In Table I we present details of the diagonalization results on the basis of $4s$-$4d$ two-state mixing only. We see that the avoided crossing occurs at $R_c \approx 1.92$ a.u. with an adiabatic curve splitting $2 \times \Delta\epsilon = 0.0004$ a.u. and a coupling region of width $\Delta R = 0.4$ a.u.

We are interested primarily in low-energy AI collisions, and the kinetic energy in the coupling region thus stems exclusively from the depth of the potential-energy curve, about 0.08 a.u. (cf. Fig. 1). The Massey criterion for adiabaticity may be formulated in terms of the relative velocity v in the near-crossing region $v \ll v_0 = \Delta\epsilon \times \Delta R$ (in a.u.). We obtain $v_0 \approx 8 \times 10^{-5}$ a.u. and $v \approx 10^{-2}$ a.u., and

TABLE I. Matrix elements, resulting adiabatic energies, and coupling coefficients in the crossing region for the $4s$-$4d$ two-state diagonalization of H_e (a.u.).

R	$\langle 4d \mid H_e \mid 4d \rangle$	$\langle 4s \mid H_e \mid 4s \rangle$	$\langle 4s \mid H_e \mid 4d \rangle$	$\epsilon^{(1)}_{(4s)\sigma}$	$\epsilon^{(1)}_{(4d)\sigma}$	$a(4s, 4d)$	$a(4s, 4s)$
1.70	−0.033 19	−0.034 12	0.000 151	−0.034 14	−0.033 17	0.156	0.988
1.80	−0.033 27	−0.033 75	0.000 174	−0.033 81	−0.033 21	0.309	0.951
1.85	−0.033 31	−0.033 60	0.000 185	−0.033 69	−0.033 22	0.438	0.899
1.90	−0.033 37	−0.033 45	0.000 197	−0.033 61	−0.033 21	0.633	0.774
1.95	−0.033 42	−0.033 28	0.000 209	−0.033 57	−0.033 13	0.584	0.812
1.975	−0.033 43	−0.033 20	0.000 212	−0.033 56	−0.033 07	0.511	0.859
2.00	−0.033 44	−0.033 10	0.000 218	−0.033 55	−0.032 99	0.439	0.899
2.05	−0.033 51	−0.032 95	0.000 229	−0.033 59	−0.032 87	0.336	0.942
2.10	−0.033 53	−0.032 80	0.000 242	−0.033 60	−0.032 73	0.289	0.957
2.15	−0.033 58	−0.032 60	0.000 257	−0.033 65	−0.032 58	0.250	0.968
2.20	−0.033 60	−0.032 50	0.000 267	−0.033 66	−0.032 44	0.224	0.975
2.30	−0.033 75	−0.032 20	0.000 291	−0.033 80	−0.032 15	0.179	0.984

hence $v \gg v_0$. The peculiarity of a near crossing at about the minimum point of the potential-energy curves (v large), only slightly separated ($\Delta\epsilon$ small), thus makes the adiabatic description invalid. Also, Landau-Zener estimates of nonadiabatic transitions show adiabatic curve switching of probabilities close to unity. Very much the same conclusion may be drawn for $3s$-$3d$, $5s$-$5d$, and $6s$-$6d$ near crossings. We have chosen therefore to represent the ns and nd σ states by the diabatic set of states, Eqs. (9) and (10), and the corresponding crossing potential-energy curves, based upon the energies of Eq. (12).

III. SCATTERING FORMULATION

We uniformly express the nuclear motion in the laboratory system and the electron motion in the molecular system. We have chosen this representation because it is the proper point of view for slow thermal collisions in the regions of phase space where AI may occur ($R \lesssim 4$ a.u.). Our basis functions are derived from the Born-Oppenheimer approximation, corresponding to the adiabatic limit. To derive these basis functions for atomic as well as ionic channels, we have included all regular R-dependent interactions except the Sternheimer interaction operator W,

$$-\frac{1}{m_H}\left[\frac{\partial^2}{\partial R^2}\,\psi_\Lambda(\vec{r}, R)\right]\left[\psi_\Lambda(\vec{r}, R)\right]^{-1}$$
$$-\frac{2}{m_H}\left[\frac{\partial}{\partial R}\,\psi_\Lambda(\vec{r}, R)\right]\left[\frac{\partial}{\partial R}\,\chi(R)\right]\left[\psi_\Lambda(\vec{r}, R)\,\chi(R)\right]^{-1}, \tag{17}$$

giving rise to transitions between the adiabatic bound-electron states and between the adiabatic free-electron states and finally between bound- and free-electron states causing the AI transition. We consider now the direct transitions from the atomic (free-nuclear bound-electronic state) channels to the ionic (bound-nuclear free-electronic state) channels as a result of the vibronic operator W. We invoke a perturbed stationary-state treatment; nonreactive scattering is described by the stationary adabatic scattering states of our model Hamiltonian with W neglected. These states are easily constructed from the states given in Sec. II.

A slight complication arises in formulating our adiabatic states as proper scattering states. The plane waves (in the ionic channels, plane Coulomb waves) and the ingoing or outgoing spherical waves to be constructed, must necessarily be referred to the same laboratory system for all channels. This is trivial for the atomic channels, but for the ionic channels we have so far (just like for the atomic channels) referred the electron motion to the molecular system. At present we are not interested in differential cross sections. Hence the scattering angle is only an integration variable and we may choose it in a way most convenient for that purpose. However, to formulate the scattering event in terms of scattering amplitudes, differential cross sections, and finally total cross sections, we must start out by formulating the scattering states in all the channels in the same frame of reference. For integration purposes we may then transform the expression for the total cross section to other frames.

Let a and i stand for the collections of quantum numbers and energies that characterize the atomic and the ionic channels of AI-DR [Eq. (1)], i.e., $a = a(nl\Lambda,\ k_a)$ and $i = i(vKM,\ k_i)$. In terms of the T-matrix elements and the density of final states we may write the differential cross section for AI in specified channels as[45]

$$q(a \to i,\ \hat{\vec{k}}_i) = \frac{2\pi m_a}{k_a}\,\left|T(a \to i,\ \hat{\vec{k}}_i)\right|^2 \rho(E_i)$$
$$= \frac{m_a m_i}{(2\pi)^2}\,\frac{k_i}{k_a}\,\left|T(a \to i,\ \hat{\vec{k}}_i)\right|^2, \tag{18}$$

$$T(a \to i,\ \hat{\vec{k}}_i) = \langle \Psi_i^{(-)} | W | \Psi_a^{(+)} \rangle, \tag{19}$$

where m_a and m_i are reduced masses in atomic and ionic channels, respectively, i.e., $m_a = \frac{1}{2}m_H$ and $m_i = 1$ a.u.

The stationary waves are defined in the atomic channels to go asymptotically ($R \to \infty$) as a plane wave plus an outgoing spherical wave,

$$\Psi_a^{(+)} = \chi_a^{(+)}(\vec{R})\,\psi_{nl\Lambda}^{(1)}(\vec{r}, R), \tag{20}$$

$$\chi_a^{(+)}(\vec{R}) = \frac{4\pi}{k_a^{1/2} R} \sum_{K'M'} \exp(i\eta_{K'} + \tfrac{1}{2} iK'\pi)$$
$$\times\, Y_{K'}^{M'*}(\hat{\vec{k}}_a)\, Y_{K'}^{M'}(\hat{\vec{R}})\,\chi_{K'}(k_a, R), \tag{21}$$

$$\psi_{nl\Lambda}^{(1)}(\vec{r}, R) = \sum_{n''l''} a(nl, n''l'', R)\, Y_{l''}^{\Lambda}(\hat{\vec{r}})\,\psi_{n''l''}^{(0)}(r, R)/r. \tag{22}$$

The function $\chi_K(k_a, R)$ denotes the regular solution of the radial equation (8a) with the asymptotic behavior given by

$$\chi_K(k_a, R) \xrightarrow[R \to \infty]{} k_a^{-1/2} \sin[k_a R - \tfrac{1}{2}\pi K + \eta_K(k_a)], \tag{23}$$

where $\eta_K(k_a)$ is the phase shift of the wave. We choose the laboratory z axis along the direction of the propagation vector of the incident atoms and the expansion (21) reduces to

$$\chi_a^{(+)}(\vec{R}) = \frac{(4\pi)^{1/2}}{k_a^{1/2} R} \sum_{K'} (2K'+1)^{1/2}$$
$$\times \exp(i\eta_{K'} + \tfrac{1}{2} iK'\pi)\, Y_{K'}^{0}(\hat{\vec{R}})\,\chi_{K'}(k_a, R). \tag{24}$$

The electronic state, Eq. (22), is identical to the one defined in Eq. (5), $\psi_{nl}^{(0)}(r, R)/r$ denoting the radial part of the solution $\psi_{nl\Lambda}^{(0)}(\vec{r}, R)$ to Eq. (3).

For the ionic channels the stationary waves are defined to go asymptotically ($r \to \infty$) as a plane (Coulomb) wave plus an incoming spherical (Coulomb) wave,

$$\Psi_i^{(-)} = \psi_i^{(-)}(\vec{r}', R)\,[Y_K^M(\hat{\vec{R}})\chi_{vK}(R)/R]\,, \tag{25}$$

where primed vectors indicate electron coordinates in the laboratory frame of reference, and

$$\psi_i^{(-)}(\vec{r}', R) = \frac{4\pi}{k_i^{1/2} r} \sum_{l'm'} i^{l'} e^{-i(\sigma_{l'}+\delta_{l'})} \times Y_{l'}^{m'*}(\hat{\vec{k}}_i') Y_{l'}^{m'}(\hat{\vec{r}}') \psi_{l'}^{(0)}(k_i, r, R)\,. \tag{26}$$

$\psi_i^{(0)}(k_i, r, R)/r$ denotes the radial part of the free regular solution to Eq. (3) with the asymptotic behavior given by

$$\psi_i^{(0)}(k_i, r, R) \underset{r\to\infty}{\longrightarrow} k_i^{-1/2} \sin[k_i r + (1/k_i)\ln(2k_i r) - \tfrac{1}{2}\pi l + \sigma_l(k_i) + \delta_l(k_i, R)]\,, \tag{27}$$

where $\sigma_l(k_i)$ is the Coulomb phase shift and $\delta_l(k_i, R)$ is the short-range (non-Coulomb) phase shift. The nuclear state, included in the brackets of Eq. (25), is the one of the hydrogen molecular-ion ground state, obtained as a solution to Eq. (8b).

Substituting these expressions for the stationary waves of proper limiting form into the T-matrix element (19), we are not able to perform the integrations and to evaluate $q(\hat{\vec{k}}_i')$ unless we transfer the coordinates of the electron from the molecular frame to the laboratory frame of reference.

We are, however, only interested in evaluating total cross sections,

$$Q_{\mathrm{AI}}(a \to i) = \frac{m_a m_i}{(2\pi)^2} \frac{k_i}{k_a} \int d\hat{\vec{k}}_i' \,|T(a \to i, \vec{k}_i')|^2\,, \tag{28}$$

and now we are able to perform the integration over all solid angles to begin with and for fixed internuclear axis. Introducing, instead of Eq. (26), an expansion of $\psi_i^{(-)}$ in the molecular frame ($\hat{\vec{k}}_i$ and $\hat{\vec{r}}$ now measured relative to $\hat{\vec{R}}$)

$$\psi_i^{(-)}(\vec{r}, R) = \frac{4\pi}{k_i^{1/2} r} \sum_{l'\Lambda'} i^{l'} e^{-i(\sigma_{l'}+\delta_{l'})} \times Y_{l'}^{\Lambda'*}(\hat{\vec{k}}_i) Y_{l'}^{\Lambda'}(\hat{\vec{r}}) \psi_{l'}^{(0)}(k_i, r, R)\,, \tag{29}$$

we may in Eq. (28) go through the integrations over $\hat{\vec{k}}_i$ and $\hat{\vec{r}}$ for fixed $\hat{\vec{R}}$, and then perform the $\hat{\vec{R}}$ integration. Finally, we are left with two radial integrations, one over r for fixed R and one over R.

For AI cross sections into molecular-ion states (v, K) irrespective of angular momentum projection, i.e., for cross sections into the degenerate set of states (v, K), we obtain

$$Q_{\mathrm{AI}}(nl\Lambda, k_a \to v, K) = \frac{16\pi}{m_a k_a^2} (2K+1) \sum_{l'} \left| \int \chi_{vK}(R) F(nl', k_i l', R) \frac{\partial}{\partial R} [a(nl, nl', R)\chi_K(k_a, R)]\, dR \right|^2\,, \tag{30}$$

$$F(nl', k_i l', R) = \int \psi_{l'}^{(0)}(k_i, r, R) \frac{\partial}{\partial R} \psi_{nl'}^{(0)}(r, R)\, dr\,, \tag{31}$$

where the summation over l' arises from the representation (22) of the bound-electron states, $ns\sigma$ and $nd\sigma$ states mixing strongly in the R region of interest. Scattering corresponding to the $ns\sigma$ and $nd\sigma$ potential-energy curves in either case may result in AI by $ns \to l' = 0$, as well as $nd \to l' = 2$ electronic transitions. In all other channels the summation is reduced essentially to one term—the fairly constant parental component of the electron state.

The two terms of the vibronic diabatic operator W (17) actually give rise to several contributions to the T-matrix element (19) when we introduce the representation of the bound-electron state $\psi_a = \sum a' \psi_{a'}^{(0)}$. Each component contributes, in a short-hand notation [cf. Eqs. (6) and (7) of Paper I],

$$T_1 = \left[\psi_i^{(0)}\chi_i \left| a(R)\left(\frac{\partial}{\partial R}\psi_a^{(0)}\right)\left(\frac{\partial}{\partial R}\chi_a\right)\right.\right] + \left[\psi_i^{(0)}\chi_i\, \psi_a^{(0)}\left(\frac{\partial}{\partial R}a\right)\left(\frac{\partial}{\partial R}\chi_a\right)\right], \tag{32}$$

$$T_2 = \tfrac{1}{2}\left[\psi_i^{(0)}\chi_i \left| a(R)\left(\frac{\partial^2}{\partial R^2}\psi_a^{(0)}\right)\chi_a\right.\right] + \tfrac{1}{2}\left[\psi_i^{(0)}\chi_i \left| \psi_a^{(0)}\left(\frac{\partial^2}{\partial R^2}a\right)\chi_a\right.\right] + \left[\psi_i^{(0)}\chi_i \left| \left(\frac{\partial}{\partial R}a\right)\left(\frac{\partial}{\partial R}\psi_a^{(0)}\right)\chi_a\right.\right]. \tag{33}$$

The second term of T_1 and the second term of T_2 vanish identically by the integration over electron

coordinates, because $\psi_a^{(0)}$ and $\psi_i^{(0)}$ are eigenfunctions of the *same* Hamiltonian. The first term of T_2, displaying a second derivative with respect to R of the electron state, may be neglected when compared to the first term of T_1, where the electronic part of the matrix element contains a first derivative with respect to R. Finally, the first term of T_1 and the third term of T_2 may be combined to a single matrix element:

$$T_1 + T_2 \approx \left\{ \psi_i^{(0)} \chi_i \middle| \left[\frac{\partial}{\partial R} \psi_a^{(0)} \right] \frac{\partial}{\partial R} \left[a(R) \chi_a \right] \right\}, \quad (34)$$

resulting in final integrations in the cross-section expression as displayed in Eqs. (30) and (31).

We note that for electron states of definite parentage, $a(R)$ is approximately a constant (≈ 1) and the over-all vibronic matrix element (34) reduces to T_1 (discussed in detail in Paper I).[46] For near-crossing states, on the other hand, $a(R)$ is a strongly varying function of R in the region of the avoided crossing; T_2 thus makes an essential contribution to the vibronic coupling, and $T_1 + T_2$ is the pertinent vibronic-coupling matrix element. However, from a computational point of view it is convenient that we do not have to evaluate the two contributions separately.

The electronic part of the matrix element, $F(nl, k_i l, R)$, may conveniently be evaluated in a form using the first derivative with respect to R of the potential $V_{0cE}(r, R)$, the results of which were discussed in Paper I. It is important that F turns out to be essentially independent of k_i for free-electron states of energies up to about 0.1 a.u.

We may finally define cross sections $Q_{\mathrm{AI}}(nl\Lambda, k_a \to v)$ for AI from definite molecular electron states into a specific vibrational state by summation of Eq. (30) over all $K \geq 0$, and also an over-all cross section $Q_{\mathrm{AI}}(nl\Lambda, k_a)$ by summation over all K and v.

Having obtained AI cross sections for channels as specified in Eq. (30), we may invoke microscopic reversibility to obtain DR cross sections in the very same channels:

$$Q_{\mathrm{DR}}(v, K, k_i \to nl\Lambda) = (k_a^2/k_i^2)\, Q_{\mathrm{AI}}(nl\Lambda, k_a \to v, K) , \quad (35)$$

i.e., cross sections for DR from the degenerate set of states (v, K) for unit flux for each degenerate state. More relevant, however, is

$$\overline{Q}_{\mathrm{DR}}(v, K, k_i \to nl\Lambda) = [1/(2K+1)]\, Q_{\mathrm{DR}}(v, K, k_i \to nl\Lambda) , \quad (36)$$

which is the cross section for DR from the degenerate set (v, K) for unit flux for the total set of degenerate states. We note that for microscopic reversibility to be fulfilled both terms of the diabatic operator are in principle required.

It is often convenient to express AI and DR results in terms of the specific rates of the reactions, for example, at room temperature. Let us assume an equilibrium distribution of translational energy, allowing us to evaluate rate constants from cross sections according to

$$k(T) = \left(\frac{8kT}{\pi m} \right)^{1/2} \int_0^\infty Q(E)\, E\, e^{-E/kT}\, \frac{dE}{(kT)^2} . \quad (37)$$

We may obtain rate constants for AI in specific channels, for example, $k_{\mathrm{AI}}(nl\Lambda \to v, K \mid T)$, $k_{\mathrm{AI}}(nl\Lambda \to v \mid T)$, and $k_{\mathrm{AI}}(nl\Lambda, T)$ using in Eq. (37) $m = m_a$ and the AI cross sections defined above, $k_a^2 = 2m_a E$. For DR we may obtain $k_{\mathrm{DR}}(v, K \to nl\Lambda \mid T)$ using in Eq. (37) $m = m_i$ and the cross section $Q_{\mathrm{DR}}(v, K, k_i \to nl\Lambda)$, $k_i^2 = 2m_i E$.

In our scattering formulation we have disregarded for simplicity the resolution of a given molecular electronic state into laboratory-quantized atomic states at large internuclear distances. The AI transition range is localized exclusively to short distances ($R \lesssim 4$ a.u.) and we have defined the scattering process in terms of unique molecular electronic states. We feel that, apart from interference effects, our model calculation accounts for the main features of the AI and DR reaction mechanism in hydrogen, giving order-of-magnitude values for reaction cross sections and rates.

IV. COMPUTATIONAL RESULTS

We have restricted the present investigation of AI for hydrogen to the H* ($n = 3$) excited atomic states. We have furthermore neglected the three $l = 3$ (f) united-atom states, i.e., the $\sigma_u(3s)$, $\sigma_u(3d)$, and $\delta_u(3d)$ separated-atom states, since the $nf \to l = 3$ electronic transitions give rise to matrix elements about two orders of magnitude less than those of the $np \to l = 1$ electronic transitions. That leaves us with a total of nine Rydberg states ($1s\sigma_g$, $nl\Lambda$) in the united-atom limit, correlating to the $n = 3$ atomic state at infinite separation. These are $3d\sigma_g[\sigma_g(3s)]$, $4s\sigma_g[\sigma_g(3p)]$, $4d\sigma_g[\sigma_g(3d)]$, $5p\sigma_u[\sigma_u(3p)]$, $4d\pi_g[\pi_g(3p)]$, $5d\pi_g[\pi_g(3d)]$, $3p\pi_u[\pi_u(3p)]$, $4p\pi_u[\pi_u(3d)]$, and $3d\delta_g[\delta_g(3d)]$, where the separated-atom configurations are given in brackets. However, as previously discussed, we choose instead of the first three mentioned the corresponding diabatic states, displaying crossings near $R = 2$ a.u., i.e., states $3s\sigma_g[\sigma_g(3s)]$, $4d\sigma_g[\sigma_g(3p)]$, and $4s\sigma_g[\sigma_g(3d)]$.

AI Rate Constants

The investigation is directed primarily towards low-energy (thermal) AI, i.e., AI in the temperature range 300–1000 °K. We have used, therefore, the specific rate constants $k_{\mathrm{AI}}(nl\Lambda \to v, K \mid T = 300\,^\circ\mathrm{K})$, Eq. (37), to give an over-all picture of the channel dependences, in particular, to identify the electronic molecular state or states that dominate the

TABLE II. For the exothermic or near-exothermic (resonance) AI channels from ($n=3$) atomic states, corresponding to molecular-ion states $H_2^+(v, K)$ of energy less than or about $-0.555\,56$ a.u., are given the molecular-ion energy $E_{v,K}$, the threshold energy $E_T = E_{v,K} + 0.555\,56$, and the rotational barrier energy for the $4s\sigma$ potential-energy curve $E_{RB}(4s\sigma)$ in a.u.

v	K	$E_{v,K}$	E_T	$E_{RB}(4s\sigma)$
6	0	−0.545 84	0.009 72	0
5	0	−0.553 09	0.002 47	0
4	6	−0.556 52	−0.000 96	0.000 13
4	7	−0.555 13	0.000 43	0.000 19
4	8	−0.553 58	0.001 98	0.000 26
3	10	−0.557 63	−0.002 07	0.000 46
3	11	−0.555 51	0.000 05	0.000 57
3	12	−0.553 27	0.002 29	0.000 72
2	13	−0.558 65	−0.003 09	0.000 88
2	14	−0.556 03	−0.000 47	0.001 06
2	15	−0.553 31	0.002 25	0.001 28
1	16	−0.558 29	−0.002 73	0.001 51
1	17	−0.555 23	0.000 33	0.001 77
0	19	−0.556 67	−0.001 11	0.002 40
0	20	−0.553 24	0.002 32	0.002 72

AI process, and then to investigate in detail cross-section behavior for the corresponding subchannels.

We designate an AI channel as exothermic (endothermic) when the energy of the molecular-ion state $E_{v,K}$ is below (above) the energy of the related stationary and separated atoms, $-0.555\,56$ a.u., and we introduce a threshold energy $E_T = E_{v,K} + 0.555\,56$. Any channel for which $E_T > 10^{-2}$ a.u. makes a negligible contribution to AI at 300 °K ($E \approx 10^{-3}$ a.u.) In Table II we have listed characteristic energies for various channels, particularly threshold energies about zero (resonance channels). All channels with $v \geq 5$ are endothermic, and the channels with $v \geq 6$ are of no importance for AI at 300 °K. Near-resonant channels are ($v=4$, $K=6$, 7), ($v=3$, $K=11$), ($v=2$, $K=14$), ($v=1$, $K=17$), and ($v=0$, $K=19$, 20). The results for the six most significant electronic channels are shown in Figs. 3(a)–3(f) by contour diagrams giving order-of-magnitude results for rate constants for AI into all possible specific vibrational-rotational states of the molecular ion.

Over-all AI rate constants $k_{AI}(nl\Lambda \to v \mid T = 300\,^\circ\mathrm{K})$ for these channels into molecular-ion vibrational states ($v \leq 5$) are given in Table III together with the total rate constants $k_{AI}(nl\Lambda,\ T = 300\,^\circ\mathrm{K})$, the electronic states ordered according to decreasing total rate constants. We see that AI by $4s\sigma$ channel and, to a lesser degree, $4d\sigma$, $5d\pi$, and $3s\sigma$ channels, dominate, by orders of magnitude, as compared to AI by any other electronic channel correlating to the ($1s\sigma_g$, $3l$) atomic states. We notice that, with only a few exceptions the ordering thus chosen is equivalent roughly to an ordering according to the magnitude of the rate into specific vibrational states as well, i. e., given $k_{AI}(nl\Lambda,\ T = 300\,^\circ\mathrm{K}) > k_{AI}(n'l'\Lambda',\ T = 300\,^\circ\mathrm{K})$, then also $k_{AI}(nl\Lambda,\ v \mid T = 300\,^\circ\mathrm{K}) > k_{AI}(n'l'\Lambda',\ v \mid T = 300\,^\circ\mathrm{K})$ for any v. We notice that $k_{AI}(nl\Lambda,\ v \mid T = 300\,^\circ\mathrm{K})$ increases with v, for $v < 5$, with one exception only, and the total rate into the vibrational states $v \geq 5$ (endothermic channels), about 1 % of the total rate, is of the order of magnitude of the rate into the $v = 0$ vibrational state. The regularity thus apparent from Table III in the rates into specfic vibrational states independent (in most cases) of electronic state persists where the rates are broken into rates for specific vibrational-rotational states [Figs. 3(a)–3(f)]. The AI rate into a given rotational state K from any electronic state $nl\Lambda$ increases rapidly with v, by order of magnitude for each vibrational quantum in exothermic channels, reaching a maximum value for (v, K) equal to or close to resonance values, and finally decreasing, often by orders of magnitude for each vibrational quantum in the endothermic channels of higher v (compare Table II). For AI into a given vibrational state of an exothermic channel (at $K = 0$), the rate increases rather slowly for increasing K, reaching maximum values often about and just below the K that makes the channel a resonance channel, and then decreasing rapidly by about an order of magnitude for each additional rotational quantum in the endothermic channels of higher K.

The general (v, K) dependence of AI rates, which is often independent of the initial electronic state, is quite apparent from the contour diagrams of Fig. 3. For closer inspection we have given in

TABLE III. Rate constants for AI from molecular electronic states $nl\Lambda$ into specific vibrational states of the molecular ion, $k_{AI}(nl\Lambda \to v \mid T = 300\,^\circ\mathrm{K})$ in units of $\mathrm{cm}^3/\mathrm{sec}$ (powers of 10 given in parentheses).

$nl\Lambda$ \ v	0	1	2	3	4	5	$\sum_v$
$4s\sigma$	1.7 (−14)	7.8 (−14)	1.3 (−13)	3.3 (−13)	4.4 (−13)	8.3 (−15)	1.0 (−12)
$4d\sigma$	2.1 (−14)	4.1 (−14)	9.0 (−14)	9.7 (−14)	4.2 (−14)	1.9 (−15)	2.9 (−13)
$5d\pi$	3.3 (−16)	6.3 (−15)	2.4 (−14)	7.4 (−14)	1.1 (−13)	2.3 (−15)	2.2 (−13)
$3s\sigma$	6.6 (−15)	1.6 (−14)	2.4 (−14)	3.0 (−14)	4.1 (−14)	1.3 (−15)	1.2 (−13)
$4d\pi$	7.0 (−17)	1.1 (−15)	4.8 (−15)	1.4 (−14)	2.5 (−14)	5.9 (−16)	4.6 (−14)
$5p\sigma$	1.6 (−16)	1.8 (−15)	1.0 (−15)	7.3 (−15)	1.8 (−14)	5.3 (−16)	2.8 (−14)

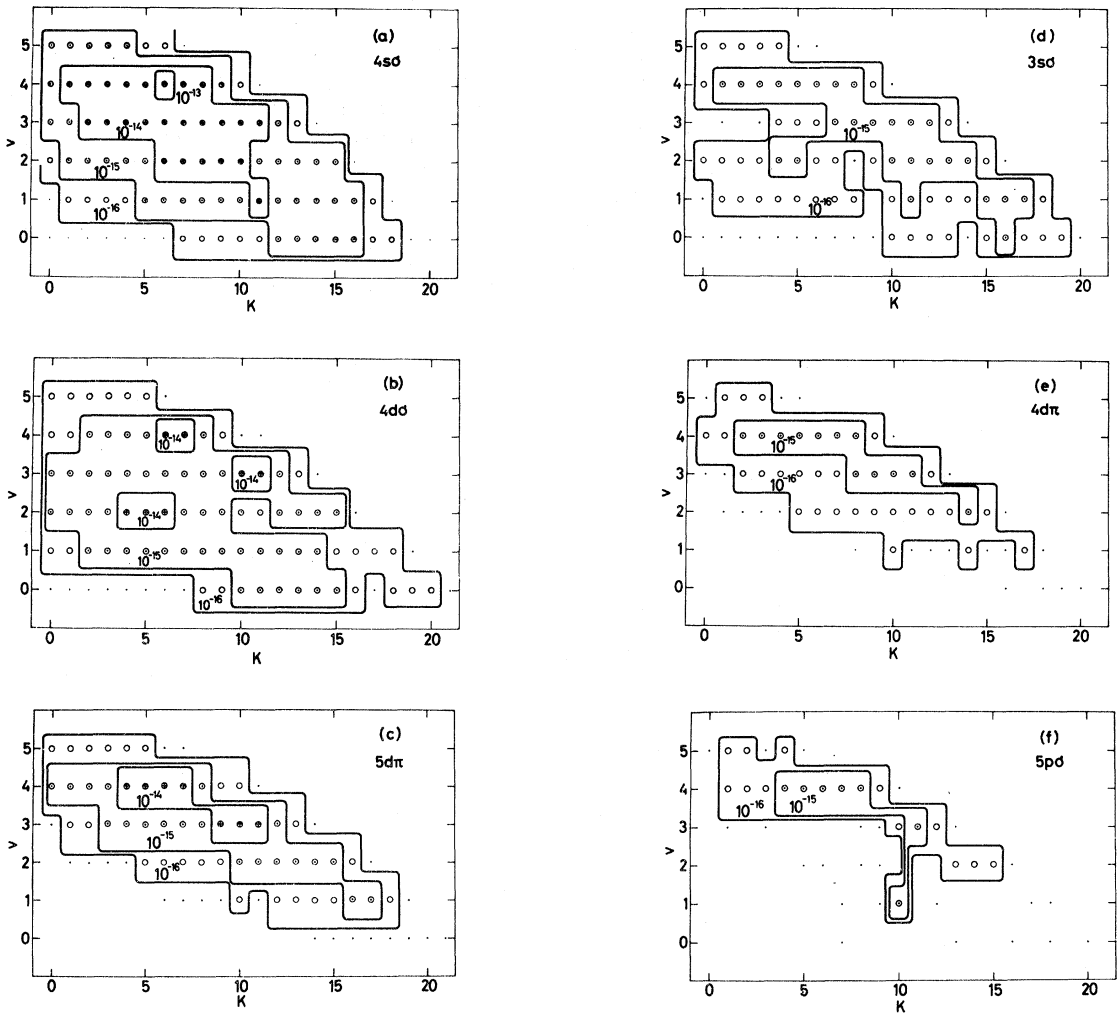

FIG. 3. Contour map of specific rates for AI, $k_{AI}(nl\Lambda \rightarrow v, K \mid T = 300\ ^\circ\mathrm{K})$, as functions of electronic state $(nl\Lambda)$, and vibrational (v) and rotational (K) state of the molecular ion. Contours represent successive factors of 10 in rates. An entry (v, K) marked by a dot indicates an AI rate in the range $10^{-17}-10^{-16}$ cm^3/sec, and an unmarked entry a rate below 10^{-17} cm^3/sec. The electronic states are (a) $4s\sigma$, (b) $4d\sigma$, (c) $5d\pi$, (d) $3s\sigma$, (e) $4d\pi$, and (f) $5p\sigma$.

Table IV the actual values of the rate constants $k_{AI}(nl\Lambda, v, K \mid T = 300\ ^\circ\mathrm{K})$ for the dominant electronic channels. We see that in general the significant (v, K) channels are those for which the threshold energies are as close to zero as possible, i.e., the resonance channels.

The differences observed in the AI rates from the possible molecular electronic states (Table III) may be ascribed first of all to the different electronic transitions involved rather than to the different potential-energy curves. The electronic matrix element $F(nl, k_i l; R)$ of Eq. (31), appearing as a weighting factor in the nuclear integration of the cross-section expression (30), differ widely in magnitude as well as in R dependence for s, p, and d transitions (Paper I). The $ns \rightarrow l = 0$ transitions are highly favored because $F(ns, k_i 0; R)$ functions are large over the entire R range, and we expect $ns\sigma$ and $nd\sigma$ channels, all having s components, to be important AI channels. As Table III shows, this is indeed the case for $4s\sigma$ and $4d\sigma$. Furthermore, we find that AI in the $4s\sigma$ and $3s\sigma$ channels is due almost entirely to the $ns \rightarrow l = 0$ transition; the $nd \rightarrow l = 2$ term of Eq. (30) contributes less than a few percent of the total rate. For the $4d\sigma$ channel, we find that AI from the more significant subchannels may derive as much as 25–50% of their values from the $4d \rightarrow l = 2$ contribution. The $4s \rightarrow l = 0$ transition, however, occurs only in a narrow R interval about $R \approx 2$ a.u. (the H_2^+ equilibrium distance), favoring transition to low vibrational states of the molecular ion. This effect is apparent from Table III; the

$4d\sigma$ rates into vibrational states $v=0$, 1, and 2 are relatively large compared with the rates into vibrational states $v=3$ and 4.

The R dependence of F for $np \rightarrow l=1$ and $nd \rightarrow l=2$ transitions is pronounced and the magnitude generally much smaller than for $ns \rightarrow l=0$ transitions, and it is not possible to make predictions concerning the relative importance of $np\sigma$, $np\pi$, $nd\pi$, and $nd\delta$ channels.

With respect to the influence of the shapes of the potential-energy curves for different $nl\Lambda$ states, we expect nuclear transitions to be favored from curves as close as possible to the molecular-ion potential-energy curve. From Table III it appears that the specific rates do satisfy $k_{AI}(5d\pi) > k_{AI}(4d\pi)$, $k_{AI}(4s\sigma) > k_{AI}(3s\sigma)$, and $k_{AI}(5p\sigma) > k_{AI}(4p\pi) > k_{AI}(3p\pi)$, while opposite inequalities do hold for the well depths of the corresponding potential-energy curves

TABLE IV. Rate constants for AI from the molecular electronic state $nl\Lambda$ into specific vibrational-rotational states of the molecular ion, $k_{AI}(nl\Lambda \rightarrow v, K \mid T=300\,^{\circ}\mathrm{K})$ in units of $\mathrm{cm}^3/\mathrm{sec}$ (powers of 10 given in parentheses).

K \ v		0	1	2	3	4	5	$\sum_v$
A $4s\sigma$	0	1.0 (−17)	9.7 (−17)	7.3 (−16)	2.5 (−15)	5.6 (−15)	1.1 (−15)	1.0 (−14)
	1	1.6 (−17)	1.7 (−16)	2.5 (−15)	7.1 (−15)	1.6 (−14)	2.0 (−15)	2.8 (−14)
	2	6.2 (−17)	5.2 (−16)	3.7 (−15)	1.3 (−14)	2.8 (−14)	1.9 (−15)	4.7 (−14)
	3	7.0 (−17)	6.3 (−16)	6.2 (−15)	1.9 (−14)	4.0 (−14)	1.6 (−15)	6.7 (−14)
	4	7.8 (−17)	8.8 (−16)	6.8 (−15)	2.5 (−14)	4.1 (−14)	1.0 (−15)	7.5 (−14)
	5	3.1 (−17)	1.3 (−15)	8.3 (−15)	3.0 (−14)	6.7 (−14)	5.3 (−16)	1.1 (−13)
	6	2.1 (−17)	2.3 (−15)	1.7 (−14)	4.6 (−14)	1.3 (−13)	1.2 (−16)	2.0 (−13)
	7	1.4 (−16)	1.6 (−15)	1.3 (−14)	4.2 (−14)	8.5 (−14)	4.7 (−17)	1.4 (−13)
	8	1.4 (−16)	1.1 (−15)	1.1 (−14)	3.3 (−14)	1.7 (−14)	2.8 (−18)	6.2 (−14)
	9	2.3 (−16)	5.7 (−15)	1.9 (−14)	6.2 (−14)	2.6 (−15)	∼0	9.0 (−14)
	10	1.1 (−16)	1.9 (−15)	1.0 (−14)	2.7 (−14)	3.0 (−16)		3.9 (−14)
	11	7.5 (−16)	3.9 (−14)	8.6 (−15)	2.0 (−14)	3.2 (−17)		6.8 (−14)
	12	1.0 (−15)	5.6 (−15)	7.8 (−15)	4.8 (−15)	∼0		1.9 (−14)
	13	1.7 (−15)	4.0 (−15)	4.7 (−15)	2.1 (−16)			1.1 (−14)
	14	1.8 (−15)	4.5 (−15)	8.1 (−15)	2.2 (−17)			1.4 (−14)
	15	1.4 (−15)	4.4 (−15)	2.4 (−15)	∼0			8.2 (−15)
	16	8.9 (−15)	3.2 (−15)	6.0 (−17)				1.2 (−15)
	17	3.7 (−16)	9.8 (−16)	6.4 (−18)				1.3 (−15)
	18	2.9 (−16)	2.6 (−17)	∼0				3.2 (−16)
	19	1.0 (−17)	2.1 (−19)					1.0 (−17)
	20	1.0 (−16)	∼0					1.0 (−16)
	21	4.5 (−18)						4.5 (−18)
	$\sum_K$	1.7 (−14)	7.8 (−14)	1.3 (−13)	3.3 (−13)	4.4 (−13)	8.3 (−15)	1.0 (−12)
B $4d\sigma$								
	0	2.0 (−17)	2.9 (−16)	1.4 (−15)	1.1 (−15)	2.0 (−16)	2.8 (−16)	3.3 (−15)
	1	6.0 (−17)	8.9 (−16)	4.2 (−15)	3.3 (−15)	7.4 (−16)	4.5 (−16)	9.6 (−15)
	2	8.6 (−17)	1.5 (−15)	6.9 (−15)	5.1 (−15)	1.3 (−15)	4.3 (−16)	1.5 (−14)
	3	9.9 (−17)	2.1 (−15)	9.0 (−15)	6.2 (−15)	2.1 (−15)	3.5 (−16)	2.0 (−14)
	4	9.0 (−17)	2.7 (−15)	1.1 (−14)	6.3 (−15)	3.5 (−15)	2.8 (−16)	2.4 (−14)
	5	6.5 (−17)	3.4 (−15)	1.2 (−14)	6.3 (−15)	6.3 (−15)	1.1 (−16)	2.8 (−14)
	6	1.8 (−17)	3.8 (−15)	1.1 (−14)	4.3 (−15)	1.1 (−14)	2.3 (−17)	3.0 (−14)
	7	1.1 (−17)	3.7 (−15)	8.1 (−15)	1.7 (−15)	1.3 (−14)	8.5 (−18)	2.7 (−14)
	8	1.4 (−16)	3.4 (−15)	4.6 (−15)	1.0 (−15)	3.4 (−15)	∼0	1.3 (−14)
	9	8.8 (−16)	4.2 (−15)	2.0 (−15)	2.0 (−15)	6.0 (−16)		1.6 (−14)
	10	1.4 (−15)	2.9 (−15)	2.2 (−16)	1.6 (−14)	9.1 (−17)		2.1 (−14)
	11	2.2 (−15)	3.0 (−15)	7.9 (−16)	3.1 (−14)	1.4 (−17)		3.7 (−14)
	12	4.1 (−15)	2.6 (−15)	3.4 (−15)	6.5 (−15)	∼0		1.7 (−14)
	13	3.0 (−15)	1.5 (−15)	4.1 (−15)	4.5 (−16)			9.1 (−15)
	14	3.8 (−15)	1.0 (−15)	9.7 (−15)	2.9 (−17)			1.5 (−14)
	15	1.3 (−15)	1.2 (−16)	1.8 (−15)	∼0			3.2 (−15)
	16	1.7 (−16)	8.2 (−16)	6.9 (−17)				1.1 (−15)
	17	6.0 (−17)	2.5 (−15)	∼0				2.6 (−15)
	18	7.7 (−16)	8.3 (−16)					1.6 (−15)
	19	9.5 (−16)	2.5 (−17)					9.8 (−16)
	20	1.5 (−15)	∼0					1.5 (−15)
	21	4.8 (−17)						4.8 (−17)
	$\sum_K$	2.1 (−14)	4.1 (−14)	9.0 (−14)	9.7 (−14)	4.2 (−14)	1.9 (−15)	2.9 (−13)

TABLE IV (*Continued*).

K \ v	0	1	2	3	4	5	$\sum_v$
C $5d\pi$							
0	~0	~0	~0	9.0 (−17)	1.0 (−15)	3.1 (−16)	1.4 (−15)
1	~0	~0	3.0 (−17)	3.0 (−16)	3.1 (−15)	5.3 (−16)	4.0 (−15)
2	~0	~0	4.0 (−17)	6.0 (−16)	5.8 (−15)	5.1 (−16)	6.9 (−15)
3	~0	~0	8.0 (−17)	1.1 (−15)	9.5 (−15)	4.2 (−16)	1.1 (−14)
4	~0	~0	9.0 (−17)	1.6 (−15)	1.2 (−14)	3.1 (−16)	1.4 (−14)
5	~0	~0	1.1 (−16)	2.3 (−15)	1.7 (−14)	1.4 (−16)	1.9 (−14)
6	~0	2.0 (−17)	2.2 (−16)	4.8 (−15)	3.2 (−14)	3.0 (−17)	3.7 (−14)
7	~0	2.0 (−17)	3.1 (−16)	5.8 (−15)	2.5 (−14)	1.0 (−17)	3.1 (−14)
8	~0	1.0 (−17)	3.2 (−16)	6.6 (−15)	6.7 (−15)	~0	1.4 (−14)
9	~0	5.0 (−17)	7.7 (−16)	1.3 (−14)	8.4 (−16)		1.4 (−14)
10	~0	5.8 (−16)	1.3 (−15)	1.6 (−14)	1.1 (−16)		1.8 (−14)
11	~0	5.0 (−17)	1.9 (−15)	1.8 (−14)	1.0 (−17)		2.0 (−14)
12	~0	1.8 (−16)	4.7 (−15)	4.1 (−15)	~0		9.0 (−15)
13	1.0 (−18)	1.1 (−16)	2.8 (−15)	2.7 (−16)			3.2 (−15)
14	2.0 (−17)	3.9 (−16)	7.9 (−15)	2.0 (−17)			8.3 (−15)
15	2.0 (−17)	6.5 (−16)	3.7 (−15)	~0			4.3 (−15)
16	4.0 (−17)	2.2 (−15)	1.2 (−16)				2.4 (−15)
17	3.0 (−17)	1.0 (−15)	1.0 (−17)				1.1 (−15)
18	7.0 (−17)	9.9 (−16)	~0				1.1 (−15)
19	5.0 (−17)	2.0 (−17)					7.0 (−17)
20	8.0 (−17)	~0					8.0 (−17)
21	2.0 (−17)						2.0 (−17)
$\sum_K$	3.3 (−16)	6.2 (−15)	2.4 (−14)	7.4 (−14)	1.1 (−13)	2.3 (−15)	2.2 (−13)
D $3s\sigma$							
0	1.1 (−17)	3.2 (−17)	1.3 (−16)	3.4 (−18)	6.0 (−16)	1.8 (−16)	9.5 (−16)
1	3.6 (−17)	3.1 (−16)	2.9 (−16)	2.9 (−17)	1.0 (−15)	3.2 (−16)	2.0 (−15)
2	1.7 (−17)	1.9 (−16)	8.5 (−16)	8.4 (−18)	2.6 (−15)	3.0 (−16)	4.0 (−15)
3	5.1 (−17)	6.8 (−16)	7.2 (−16)	8.2 (−17)	4.0 (−15)	2.7 (−16)	5.8 (−15)
4	3.9 (−17)	4.3 (−16)	1.3 (−15)	2.7 (−16)	3.4 (−15)	1.2 (−16)	5.6 (−15)
5	6.3 (−17)	3.3 (−16)	1.0 (−15)	3.6 (−16)	9.2 (−15)	7.9 (−17)	1.1 (−14)
6	3.4 (−17)	2.7 (−16)	3.7 (−16)	4.8 (−16)	8.9 (−15)	1.8 (−17)	1.0 (−14)
7	3.1 (−17)	3.7 (−16)	1.3 (−16)	2.9 (−15)	9.0 (−15)	7.9 (−18)	1.2 (−14)
8	2.1 (−17)	2.8 (−16)	4.4 (−17)	3.5 (−15)	2.0 (−15)	~0	5.8 (−15)
9	8.7 (−17)	1.2 (−18)	3.2 (−16)	6.6 (−15)	3.6 (−16)		7.4 (−15)
10	3.1 (−16)	2.2 (−17)	1.8 (−15)	9.8 (−15)	4.6 (−17)		1.2 (−14)
11	2.4 (−16)	7.0 (−15)	4.4 (−15)	3.0 (−15)	6.8 (−18)		1.5 (−14)
12	5.1 (−16)	1.5 (−16)	4.3 (−15)	2.7 (−15)	~0		7.7 (−15)
13	3.3 (−16)	2.3 (−16)	4.0 (−15)	1.2 (−16)			4.7 (−15)
14	3.9 (−17)	2.2 (−16)	3.3 (−15)	1.3 (−17)			3.6 (−15)
15	3.7 (−16)	1.5 (−15)	6.5 (−16)	~0			2.5 (−15)
16	2.5 (−15)	1.8 (−15)	1.2 (−17)				4.3 (−15)
17	9.0 (−16)	2.0 (−15)	3.0 (−18)				2.9 (−15)
18	2.0 (−16)	1.1 (−16)	~0				3.1 (−16)
19	7.3 (−16)	2.7 (−18)					7.3 (−16)
20	7.2 (−17)	~0					7.2 (−17)
21	~0						0
$\sum_K$	6.6 (−15)	1.6 (−14)	2.4 (−14)	3.0 (−14)	4.1 (−14)	1.3 (−15)	1.2 (−13)

(cf. Paper I). For states of high n, however, the electronic factors F must ultimately vary as n^{-3}, so that for sufficiently high states, the AI rates should decrease just as the autoionization rates do (Paper II).

AI Cross Sections

For the dominant molecular electronic channel ($4s\sigma$) we show in Fig. 4 ($K = 0$–15) cross sections $Q_{AI}(4s\sigma,\ E \to v,\ K)$ in the low-energy range $0 < E < 3.5\times10^{-3}$ a.u. Maximum AI cross sections are

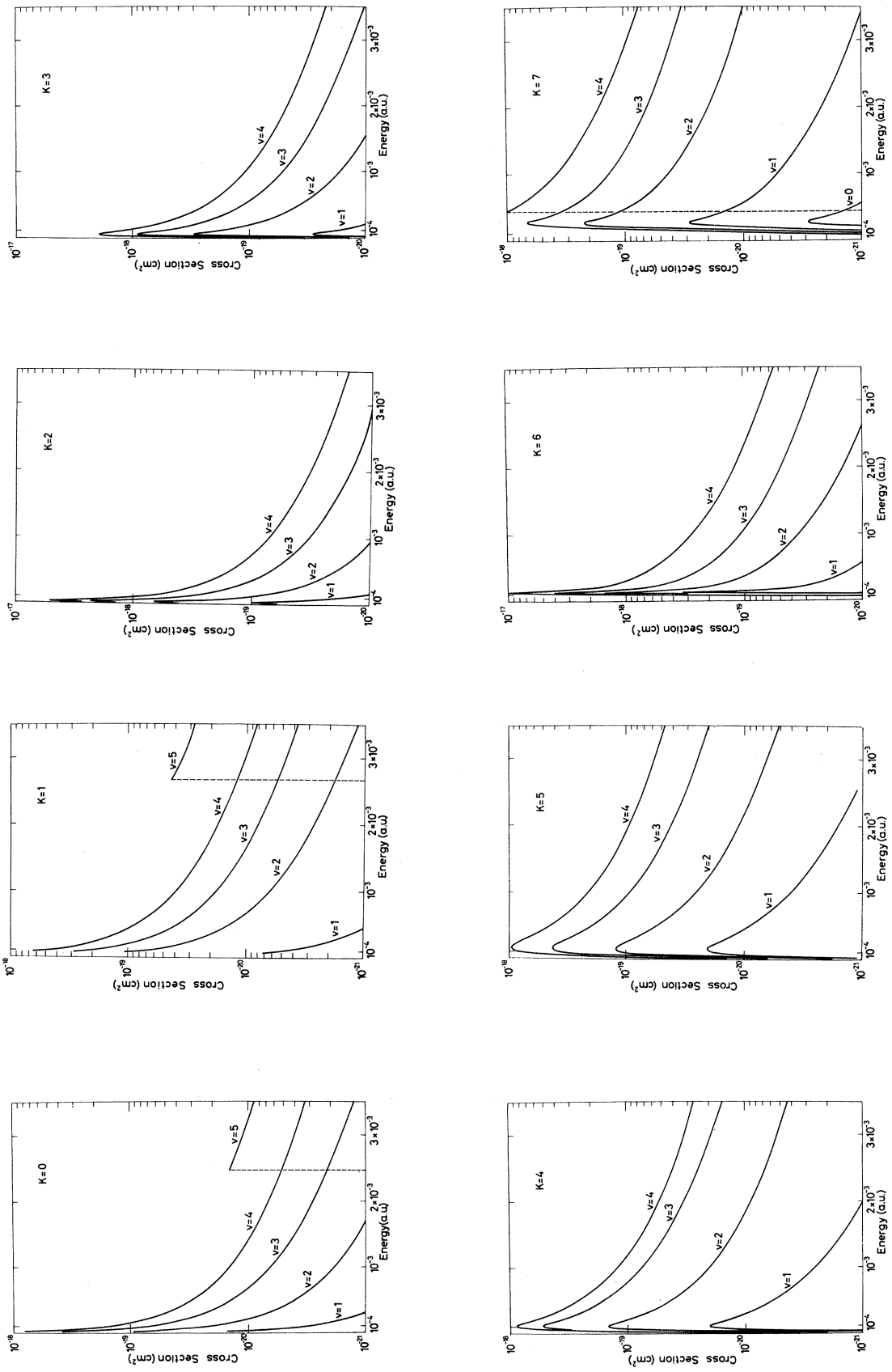

FIG. 4. Cross sections $Q_{AI}(4s\sigma,\ E \rightarrow v,\ K)$ for AI in exothermic (and near-exothermic) channels as functions of energy (E), and vibrational (v) and rotational (K) state of the molecular ion, each graph for a specific K value, $0 \leq K \leq 15$. For $K=6$ and $v=4$ the cross section reaches 1.6×10^{-17} cm^2 at $E=1.3\times10^{-4}$ a.u. For $K=11$ a sharp resonance appears at $E=3.3\times10^{-4}$ a.u., and the cross-section values (cm^2) are 7.8×10^{-18} ($v=1$), 4.5×10^{-18}($v=3$), 1.6×10^{-18}($v=2$), 1.6×10^{-19}($v=0$). For $K=14$ a sharp resonance appears at $E=9.6\times10^{-4}$ a.u., and the cross-section values (cm^2) are 1.4×10^{-18}($v=2$), 5.0×10^{-19}($v=1$), 1.7×10^{-19}($v=0$).

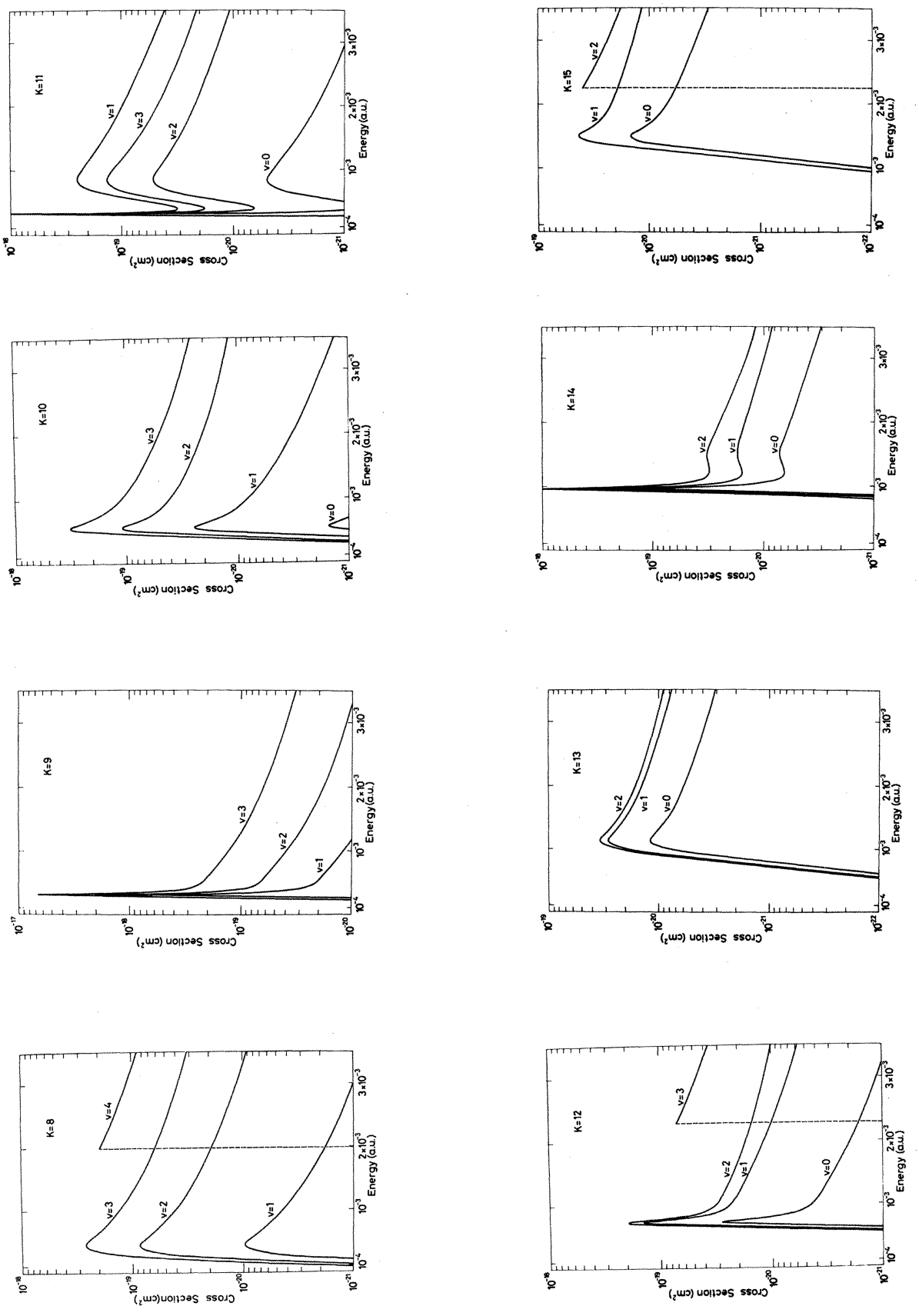

FIG. 4 (*Continued*).

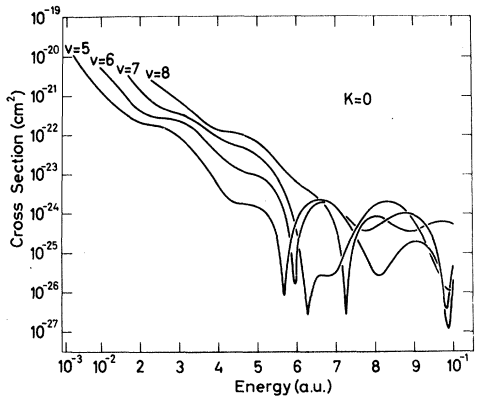

FIG. 5. Cross sections $Q_{AI}(4s\sigma,\ E \rightarrow v,\ K=0)$ for AI in endothermic channels as functions of energy (E) and vibrational state (v) of the molecular ion.

obtained in the near-resonant channels: about 10^{-17} cm^2 for $(v,\ K)=(4,\ 6)$ and $E \approx E_{RB}=1.3\times10^{-4}$ a.u.; about 10^{-18} cm^2 for $(v,\ K)=(3,\ 11)$ and $(2,\ 14)$.

In exothermic channels without rotational barriers, Q_{AI} displays a steady decrease with increasing energy according to, approximately, the power law $Q_{AI}(E)\sim E^{-\alpha}$. In exothermic channels with rotational barriers, Q_{AI} displays two different types of behavior. In the tunneling region $0<E<E_{RB}$, Q_{AI} shows an exponential rise with energy, $Q_{AI}(E) \sim e^{\beta E}$ for $E<E_{RB}$, and a maximum is reached just about or above E_{RB}. For $E>E_{RB}$ a steady decrease follows according to the power law $Q_{AI}(E)\sim E^{-\alpha}$. In endothermic channels $E_T>E_{RB}$, $Q_{AI}(E)$ decreases from a maximum at threshold according to a slow power law.

We have given in Fig. 5 the cross sections for AI into the highly endothermic channels ($K=0$) $v=5$, 6, 7, and 8. The decrease with increasing E is steady from $Q_{AI}(E_T)\approx10^{-20}$ cm^2 until about 6×10^{-2} a.u. above threshold, when undulations keep the cross sections in the range 10^{-26}–10^{-24} cm^2 up to $E\approx10^{-1}$ a.u.

The results for AI of Figure 5 may be compared with the semiempirical calculation of Chen and Peacher[34] for associative detachment (AD) of hydrogen. The over-all behavior of AI cross sections [from H + H* ($n=3$)] is very much like the behavior reported for AD cross sections in about the same energy range. The higher vibrational states of the residual molecular ion are more likely to be populated than the lower states, giving rise to an inverted population. Numerically, AI cross sections are one to two orders of magnitude smaller than those for AD (from H + H$^-$), just as one expects from the much longer range of interaction in the entrance channel for AD. The endothermic channels are essentially closed, however, in thermal AI, and their contribution to total rates may be neglected.

The over-all picture of AI from the $4s\sigma$ molecular electronic state that one obtains from the specific cross sections $Q_{AI}(4s\sigma,\ E \rightarrow v,\ K)$ does seem rather complex, and one might well doubt whether a monotonic E dependence for the total cross section $Q_{AI}(4s\sigma, E)$ may ever result. We have added the specific cross sections for each energy and plotted the result in a log-log graph against E (Fig. 6). We see that we may represent the energy dependence approximately by a power law for energies in the range $2\times10^{-4}<E<10^{-2}$ a.u., namely, $Q_{AI}(4s\sigma, E)\sim E^{-0.83}$, which is pertinent for thermal AI at about 300 °K. In the energy region below 2×10^{-4} a.u., a linear approximation is much less reliable and will give a considerably lower exponent. Using Eq. (37) we extract from the cross-section energy dependence the temperature dependence of the rate constant, and we find

$$k_{AI}(4s\sigma,\ T)\sim T^{-0.33}\ . \tag{38}$$

We may check this result by comparing with a detailed calculation of $k_{AI}(4s\sigma \rightarrow v,\ K \mid T=600\ ^\circ\text{K})$ analogous to the one already given for $T=300$ °K. The result for the total rate is $k_{AI}(4s\sigma,\ T=600\ ^\circ\text{K}) = 7.7\times10^{-13}$ cm^3/sec, i.e., $k_{AI}(4s\sigma,\ T=300\ ^\circ\text{K})/k_{AI}(4s\sigma,\ T=600\ ^\circ\text{K})\approx1.28$, where the power law given, Eq. (38), would predict the ratio to be $2^{0.33}\approx1.26$. The power law (38) thus seems reliable at temperatures 300–600 °K.

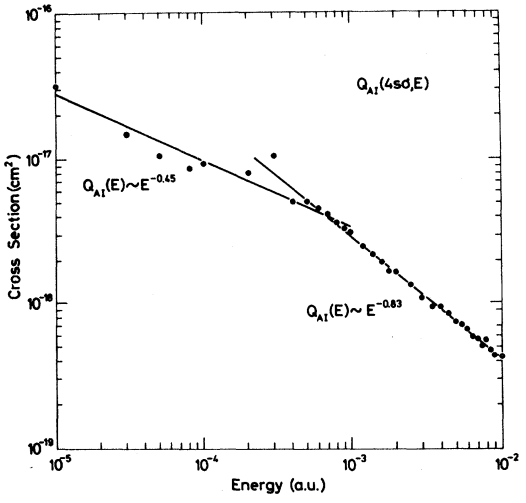

FIG. 6. Total cross section $Q_{AI}(4s\sigma,\ E)$ for AI as a function of energy in the low-energy (thermal) region. The heavy dots are the calculated values and the straight lines are linear approximations representing the power laws indicated.

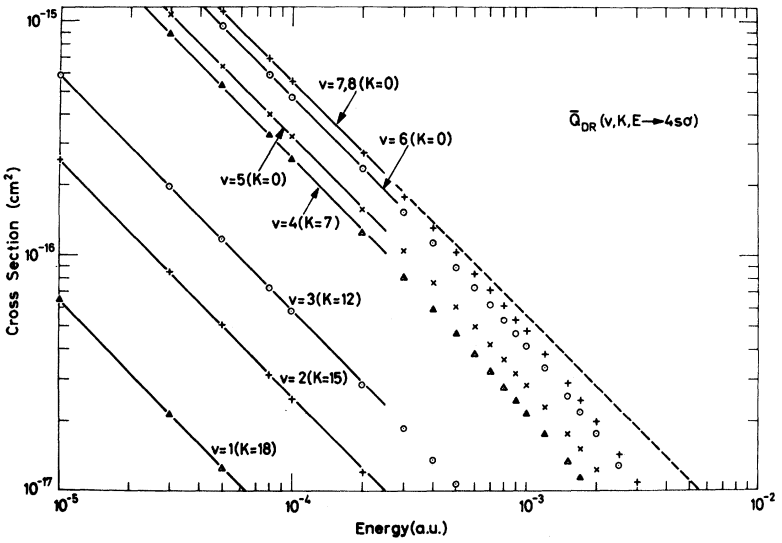

FIG. 7. Cross section $\overline{Q}_{DR}(v, K, E \rightarrow 4s\sigma)$ for DR in exothermic channels as functions of energy (E) and vibrational state (v), in each case for the lowest K value possible. The points are the calculated values and the straight lines (of slope -1) are linear approximations in the low-energy range.

DR Cross Sections and Rates

From microscopic reversibility, we have obtained cross sections for DR, the reverse of the AI process, in the same channels for which Q_{AI} was determined, Eqs. (35) and (36). In Fig. 7 we present a log-log graph of $\overline{Q}_{DR}(v, K, E \rightarrow 4s\sigma)$ for $1 \leq v \leq 8$, in each case for the K value that makes the channel open at thermal energies. The low-energy behavior is in all cases a strict $\overline{Q}_{DR}(E) \sim E^{-1}$ dependence for $E \lesssim 2\times10^{-4}$ a.u., resulting in a low-temperature rate constant (T_e is the electron temperature)

$$k_{DR}(T_e) \sim T_e^{-1/2} \quad \text{for } T_e < 80\,^{\circ}\text{K}. \tag{39}$$

This is in agreement with Wigner's threshold law for an exothermic process with a Coulomb force.[47]

In the thermal range 300–600 °K, a power law for $\overline{Q}_{DR}(E)$ is but a rough approximation. For all vibrational channels the decay of $\overline{Q}_{DR}(v, K, E)$ with energy increases for $E > 2\times10^{-4}$ a.u. In Fig. 8 we have indicated in a log-log graph a straight-line approximation to $\overline{Q}_{DR}(E)$ in an energy range about 10^{-3} a.u. on the basis of the lowest all-K exothermic DR channel ($v = 5$, $K = 0$). The power law estimated is $\overline{Q}_{DR}(E) \sim E^{-1.25}$, and the temperature dependence of the rate constant, Eq. (37), follows as

$$k_{DR}(T_e) \sim T_e^{-0.75} \quad \text{for } T_e \approx 300\text{–}600\,^{\circ}\text{K}. \tag{40}$$

At higher temperatures the power-law approximation will result in even larger exponents γ, $k_{DR}(T_e) \sim T_e^{-\gamma}$.

We conclude that the energy dependence usually adopted for DR cross sections, viz., $\overline{Q}_{DR}(E) \sim E^{-1}$, holds only in an energy region well below thermal energies ($E < 2\times10^{-4}$ a.u.), and that a faster decrease with energy, $\overline{Q}_{DR}(E) \sim E^{-\nu}(\nu > 1)$, characterizes all vibrational-rotational states about and above thermal energies ($E \gtrsim 10^{-3}$ a.u.). The resulting temperature dependence of the rate constants $k_{DR} \sim T_e^{-\gamma}(0.5 \leq \gamma \leq 0.8)$ is in agreement with most of the experimental results reported, which often show a deviation from the $T_e^{-1/2}$ behavior of just that magnitude.

We have listed in Table V DR cross sections for selected vibrational-rotational states. We notice the faster decrease with energy for $E > 10^{-4}$ a.u. of about the same magnitude for all states. We

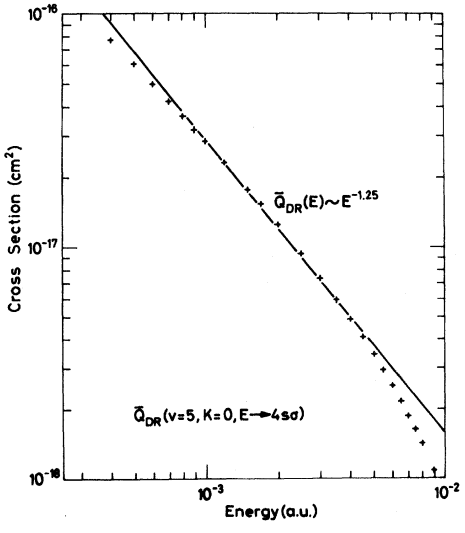

FIG. 8. Cross section $\overline{Q}_{DR}(v=5, K=0, E \rightarrow 4s\sigma)$ for DR as a function of energy in the intermediate range, $3\times10^{-4} < E < 10^{-2}$ a.u. The points are the calculated values and the straight line indicates a possible power-law representation.

TABLE V. Cross sections $\bar{Q}_{DR}(v, K, E \to 4s\sigma)$ for DR in units of 10^{-16} cm^2; energies in a.u.

v	K \ E	10^{-5}	10^{-4}	10^{-3}	10^{-2}
8	0	56	5.5	0.48	0.013
7	0	56	5.5	0.46	0.011
6	0	48	4.7	0.41	0.0078
5	0	32	3.2	0.28	0.0084
8	7	36	3.5	0.31	0.011
7	7	39	3.8	0.31	0.0083
6	7	38	3.7	0.30	0.0054
5	7	32	3.2	0.28	0.0051
4	7	27	2.6	0.22	0.0064
4	12	9.3	0.91	0.077	0.0034
3	12	5.9	0.58	0.050	0.0016
3	15	4.6	0.45	0.035	0.0005
2	15	2.6	0.25	0.020	0.0009
2	17	1.8	0.18	0.017	0.0004

observe a weak v dependence, with slightly increasing cross sections for increasing v and the same K value. For increasing K the cross section displays a weak decrease for the upper (exothermic) v channels, and a more pronounced decrease with increasing K for the lower (basically endothermic) v channels. The weak K dependence is expected since we have explicitly introduced into the model K conservation. The slight increase in DR cross sections for increasing v is of particular interest. In his discussion of DR under favorable crossing conditions, "maximal systems," O'Malley[25] argued that $Q_{DR}(v)$ falls off rapidly with increasing v (ground-state model). For systems with no favorable crossing, like the present H_2^+/H_2 system, he suggests on the basis of Franck-Condon arguments a specific $v \gg 0$ as the dominant channel for DR. We find for "nonmaximal systems" that actually a number of excited vibrational states may offer about equally effective channels for DR, in particular, when open at low K values.

For a cross-section power law we may evaluate exactly the resulting specific rate according to Eq. (37). Let us define ($E_0 = kT_e$)

$$\bar{Q}_{DR}(E) = \bar{Q}_{DR}(E_0)\,(E_0/E)^{\nu(E_0)} . \tag{41}$$

The power $\nu(E_0)$ is slightly dependent upon the energy region considered:

$$\begin{aligned} E_0 &\lesssim 2\times10^{-4}\ \text{a.u.} \quad (T_e \lesssim 80\,^\circ\text{K}), \quad \nu = 1 \\ &\approx 10^{-3}\ \text{a.u.} \quad (T_e \approx 300\,^\circ\text{K}), \quad \nu \approx 1.25 \\ &> 10^{-3}\ \text{a.u.} \quad (T_e > 300\,^\circ\text{K}), \quad \nu > 1.25 \end{aligned} \tag{42}$$

and we obtain ($\nu < 2$)

$$k_{DR}(T_e) = (8kT_e/\pi m_e)^{1/2}\,\Gamma(2-\nu)\,\bar{Q}_{DR}(kT_e) . \tag{43}$$

Using the estimate $\nu \approx 1.25$ for the energy region of thermal interest and the DR cross section obtained for the ($v = 5$, $K = 0$) molecular-ion state,

$$\bar{Q}_{DR}(v=5,\ K=0,\ E_0 = 10^{-3}\ \text{a.u.} \to 4s\sigma) = 2.8\times10^{-17}\ \text{cm}^2 ,$$

we find

$$k_{DR}(v=5,\ K=0,\ T_e = 300\,^\circ\text{K}) = 3.6\times10^{-10}\ \text{cm}^3/\text{sec}.$$

We have obtained this value on the basis of the coupling to the $4s\sigma$ Rydberg state only, the dominant channel, according to our calculation, correlating to the $n = 3$ level of the separated atoms. We may consider 3×10^{-10} cm^3/sec as a lower limit to the DR rate constant from a specific vibrational state of the molecular ion, offering exothermic low-K DR channels.

The Rydberg-state model that we have invoked in describing the excited electron states did not allow a general treatment of the states correlating to the $n = 2$ level of the separated atoms ($E = -0.625$ a.u.). These states represent nonmaximal systems and may offer DR channels as effective as the ones considered, in particular, channels of low v (ground-state molecular ion) now open for all K. For predissociation[2] we have argued that channels correlating to $n = 2$ states of the separated atoms may be neglected because of the considerable change of molecular momentum involved.

The reported v dependence of the DR cross sections does support this argument [cf. (Table V) the slight increase in rates with increasing v, i.e., with decrease in the relative change in kinetic energy in the transition region $R \approx 2$ a.u.]. We have evaluated for the $K = 0$ states the relative increase in nuclear momentum to about 20% for $v = 8$ and to about 30% for $v = 5$, for DR ($E = 10^{-3}$ a.u.) to the $4s\sigma$ state, to be compared with the DR cross sections 0.48×10^{-16} cm^2 and 0.28×10^{-16} cm^2, respectively. Indeed the results of Table V all display qualitatively (for each K series) that DR cross sections ($E \approx 10^{-3}$ a.u.) are inversely proportional to the relative increase in nuclear momentum in the transition region. For the $3d\sigma$ state, in our diabatic description an electronic state correlating to the $n = 2$ level of the separated atoms, we estimate the relative increase in nuclear momentum for DR from the ground state ($v = 0$, $K = 0$) of the molecular ion of the order 200%. Accordingly, we expect a cross section of no more than 4×10^{-18} cm^2 at $E = 10^{-3}$ a.u., and from Eq. (43) a specific rate about or less than 5×10^{-11} cm^3/sec at $T_e = 300\,^\circ$K for DR from the H_2^+ vibrational-rotational ground state.

One further point regarding the relationship between AI and DR should be recognized explicitly. Although microscopic reversibility is of course

valid and useful for relating these two complementary processes, the real processes of AI and DR will often appear to be different under realistic experimental conditions. The reason lies in the different initial states one would normally use to study the two processes. Unless pains were taken to do otherwise, the most readily prepared initial states for studying DR would be likely those with the largest Franck-Condon factors, or the thermally populated states. These are all moderately low vibrational states of H_2^+, for which the DR cross sections are small. Thermal collisions of $H(3l) + H(1s)$, by contrast, have their largest AI cross sections for $H_2^+(v = 5 - 7)$. Hence experimental studies of the two processes are likely to explore different parts of the phase space of the system.

V. CONCLUSION

The present investigation of AI and DR in hydrogen has been restricted to Rydberg states involving attractive potential-energy curves offering no crossings with the potential-energy curve of the molecular ion, i.e., to the so-called nonmaximal systems. Helium ($He + He^*$) may be another such system.

We conclude that AI in channels correlating to the $n = 3$ state of the separated atoms may occur with rates up to 10^{-12} cm^3/sec, about two orders of magnitude less than the experimental values reported for helium.[29] The cross-section energy dependence $E^{-0.83}$ compares well with the energy dependence reported for the analogous reaction $H_2 + H^* \rightarrow H_3^+ + e$.[32] AI is a typical threshold reaction, preferably occuring in near-resonance channels, leaving the free electron with low energy, and resulting in a population inversion of the vibrational states of the resulting molecular ion.

DR is favored from vibrationally excited states of the molecular ion, $v = 5$, 6, 7, 8, in channels correlating to the $n = 3$ state of the separated atoms. The rates increase slightly with v, and their magnitude, about 3×10^{-10} cm^3/sec, is considerably smaller than values estimated in previous model calculations for ground-state DR in hydrogen. Extrapolation of the results to ground-state DR in channels correlating to the $n = 2$ state of the separated atoms gives an estimated upper bound to the rate about 5×10^{-11} cm^3/sec, about the magnitude of current experimental values for DR in helium. We conclude that DR in hydrogen (and presumably in helium) may be accounted for by the noncrossing nonmaximal channels. The presence of vibrationally excited states $0 < v \leq 8$ does increase the role of DR in thermal electron recombination for these systems. However, other modes of recombination, for example, collisional radiative recombination, may still be competitive.

ACKNOWLEDGMENTS

This work was supported in part by the National Science Foundation under Grant No. GP-5535. Most of the computations were performed at Northern Europe University Computing Center, Lyngby, Denmark. We are indebted to this center for providing us with computer time and facilities.

[1]R. S. Berry and S. E. Nielsen, Phys. Rev. A 1, 383 (1970); referred to as Paper I.

[2]R. S. Berry and S. E. Nielsen, Phys. Rev. A 1, 395 (1970); referred to as Paper II.

[3]S. E. Nielsen and R. S. Berry, in *Proceedings of the Sixth International Conference on Atomic Collisions* (MIT Press, Boston, 1969), p. 1047.

[4]D. R. Bates, Phys. Rev. 77, 718 (1950); 78, 492 (1950).

[5]For general summary of the experimental and theoretical aspects of DR and AI the reader is referred to several reviews: D. R. Bates and A. Dalgarno, in *Atomic and Molecular Processes*, edited by D. R. Bates (Academic, New York, 1962), Chap. 7; J. B. Hasted, *Physics of Atomic Collisions* (Butterworths, London, 1964), Chap. 7; E. W. McDaniel, *Collision Phenomena in Ionized Gases* (Wiley, New York, 1964), Chap. 12; M. A. Biondi, in *Proceedings of the Symposium on Laboratory Measurements of Aeronomic Interest* (York University, Toronto, 1968), pp. 1–17; and R. S. Berry, in *Molecular Beams and Reaction Kinetics*, Course 44 of *International School of Physics "Enrico Fermi,"* edited by C. Schlier (Academic, New York, 1970).

[6]F. J. Mehr and M. A. Biondi, Phys. Rev. 176, 322 (1968).

[7]C. L. Chen, C. C. Leiby, and L. Goldstein, Phys. Rev. 121, 1391 (1961); H. J. Oskam and V. R. Mittelstadt, *ibid.* 132, 1445 (1963).

[8]K. B. Persson and S. C. Brown, Phys. Rev. 100, 729 (1955).

[9]W. W. Robertson, J. Chem. Phys. 42, 2064 (1965).

[10]C. B. Collins and W. W. Robertson, J. Chem. Phys. 43, 4188 (1965).

[11]C. B. Collins, Phys. Rev. 140, A1850 (1965).

[12]E. E. Ferguson, F. C. Fehsenfeld, and A. L. Schmeltekopf, Phys. Rev. 138, A381 (1965).

[13]G. K. Born, Phys. Rev. 169, 155 (1968).

[14]D. R. Bates, A. E. Kingston, and R. W. P. McWhirter, Proc. Roy. Soc. (London) A267, 297; A270, 155 (1962).

[15]R. S. Mulliken, Phys. Rev. 136, A962 (1964).

[16]S. E. Nielsen and J. S. Dahler, J. Chem. Phys. 45, 4060 (1966).

[17]P. J. Redmond, in *Proceedings of the Fifth International Conference on the Physics of Electronic and Atomic Collisions, Leningrad*, 1967 (Leningrad Nauka Publishing House, Leningrad, USSR, 1967), pp. 346–48.

[18]J. C. Y. Chen and M. H. Mittleman, Phys. Rev. 174, 185 (1968).

[19]E. Bauer and T. Y. Wu, Can. J. Phys. 34, 1436 (1956).

[20]R. Wilkins, J. Chem. Phys. 44, 1884 (1966).

[21]C. S. Warke, Phys. Rev. 144, 120 (1966).
[22]F. T. Chan, J. Chem. Phys. 49, 2533 (1968).
[23]J. N. Bardsley, Proc. Phys. Soc. (London) 1, 365 (1968).
[24]G. V. Dubrovsky, V. D. Ob'edkov, and R. K. Janev, Ref. 17, pp. 342–45.
[25]T. F. O'Malley, Phys. Rev. 185, 101 (1969).
[26]J. A. Hornbeck and J. P. Molnar, Phys. Rev. 84, 621 (1951).
[27]R. S. Berry, Ann. Rev. Phys. Chem. 20, 357 (1969).
[28]See, e.g., J. S. Dahler, J. L. Franklin, M. S. B. Munson, and F. H. Field, J. Chem. Phys. 36, 3332 (1962), and references therein.
[29]W. Kaul, P. Seyfried, and R. Taubert, Z. Naturforsch. 18a, 432 (1963).
[30]P. M. Becker and F. W. Lampe, J. Chem. Phys. 42, 3857 (1965).
[31]M. P. Teter, F. E. Niles, and W. W. Robertson, J. Chem. Phys. 44, 3018 (1966).
[32]W. A. Chupka, M. E. Russell, and K. Refaey, J. Chem. Phys. 48, 1518 (1968).
[33]R. K. Curran, J. Chem. Phys. 38, 2974 (1963).
[34]J. C. Y. Chen and J. L. Peacher, Phys. Rev. 168, 56 (1968).
[35]E. R. Davidson, in *Physical Chemistry III*, edited by H. Eyring, D. Henderson, and W. Jost (Academic, New York, 1969), Chap. 3.
[36]W. Kolos, Intern. J. Quantum Chem. II, 471 (1968).
[37]W. Kolos and L. Wolneiwicz, J. Chem. Phys. 50, 3228 (1969).
[38]W. Kolos and L. Wolneiwicz, J. Chem. Phys. 48, 3672 (1968).
[39]W. Kolos and L. Wolneiwicz, J. Chem. Phys. 45, 509 (1966).
[40]W. Kolos and L. Wolneiwicz, J. Chem. Phys. 43, 2429 (1965).
[41]J. N. Bardsley, Chem. Phys. Letters 1, 229 (1967).
[42]G. H. Dunn and B. Van Zyl, Phys. Rev. 154, 40 (1967).
[43]J. M. Peck, Phys. Rev. 154, 52 (1967).
[44]At 1000 °K, the Boltzmann factor for the seventh vibrational state of H_2^+ is 5×10^{-3}, compared with 5×10^{-2} for the state $v=2$. Hence, if the electronic-coupling crossing-point mechanism introduced by Bates were significant in the DR of $H_2^+ + e$, the mean cross section for the process would have to be at least six orders of magnitude larger than that of the noncrossing vibronic mechanism discussed here. As the results will show, this would imply that the cross section for the Bates mechanism would have to be at least $10^{-12}\,\mathrm{cm}^2$, for states with $v\geq 7$, or that the rate coefficient for DR of H_2^+ in high vibrational states would be of order 4×10^{-6}. This is between one and two orders of magnitude larger than any rate coefficient previously attributed to DR by the Bates mechanism.
[45]A. Messiah, *Quantum Mechanics* (North-Holland, Amsterdam, 1962), Vol. II, Chap. XIX.
[46]The following misprints in Paper I should be corrected: In the graphs of the transition amplitude integrals $T_1(R)$ (Figs. 2 and 3) multiply the ordinate values by a factor $\frac{1}{16}$.
[47]E. P. Wigner, Phys. Rev. 73, 1002 (1948).

PHYSICAL REVIEW A VOLUME 4, NUMBER 3 SEPTEMBER 1971

f Values for Transitions between the Low-Lying *S* and *P* States of the Helium Isoelectronic Sequence up to $Z = 10$*

B. Schiff
Department of Mathematical Sciences, Tel-Aviv University, Ramat Aviv, Israel

and

C. L. Pekeris and Y. Accad
Department of Applied Mathematics, The Weizmann Institute, Rehovot, Israel
(Received 11 January 1971)

f values have been computed for the transitions m^1S–n^1P, $m=1$–5, $n=2$–5 and m^3S–n^3P, $m,n=2$–5 for members of the helium isoelectronic sequence up to $Z=10$. The agreement between the results obtained using the dipole length, and velocity formulas, together with the convergence of the results as an increasing number of terms are included in the expansions of the wave functions, indicate that the values obtained are accurate to within 1% or better for the large majority of the transitions.

Various authors have computed *f* values for transitions between *S* and *P* states of helium and of heliumlike atoms using different types of approximate wave functions.[1–7] The wide variation between the results of the different calculations show the computed *f* values to be particularly sensitive to the wave function employed. Thus in order to obtain reasonably reliable *f* values it is necessary to employ wave functions of high accuracy. We have previously[8] obtained accurate wave functions for the states $1\,^1S$ and $n\,^1S$, $n\,^3S$, $n\,^1P$, $n\,^3P$, $n=2$–5, for members of the helium isoelectronic sequence up to $Z=10$, and have therefore been able to carry out a systematic calculation of the *f* values for